Lytic transglycosylases mitigate periplasmic crowding by degrading soluble cell wall turnover products

Anna Weaver[1,2], Laura Alvarez[3], Kelly Rosch[1], Asraa Ahmed[1,6] Garrett Wang[1], Michael VanNieuwenhze[4,5], Felipe Cava[3a], and Tobias Dörr[1,2,6a]

[1] Weill Institute for Cell and Molecular Biology, Cornell University, Ithaca, NY 14853, USA
[2] Department of Microbiology, Cornell University, Ithaca NY 14853, USA
[3] The Laboratory for Molecular Infection Medicine Sweden (MIMS), Department of Molecular Biology, Umeå University, 90187 Umeå, Sweden.
[4] Department of Molecular and Cellular Biochemistry, Indiana University, Bloomington, IN 47405, USA
[5] Department of Chemistry, Indiana University, Bloomington, IN 47405, USA
[6] Cornell Institute of Host-Microbe Interactions and Disease, Cornell University, Ithaca NY 14853, USA

[a] corresponding authors: tdoerr@cornell.edu, felipe.cava@umu.se

Abstract

The peptidoglycan cell wall is a predominant structure of bacteria, determining cell shape and supporting survival in diverse conditions. Peptidoglycan is dynamic and requires regulated synthesis of new material, remodeling, and turnover – or autolysis – of old material. Despite exploitation of peptidoglycan synthesis as an antibiotic target, we lack a fundamental understanding of how peptidoglycan synthesis and autolysis intersect to maintain the cell wall. Here, we uncover a critical physiological role for a widely misunderstood class of autolytic enzymes, lytic transglycosylases (LTGs). We demonstrate that LTG activity is essential to survival by contributing to periplasmic processes upstream and independent of peptidoglycan recycling. Defects accumulate in *Vibrio cholerae* LTG mutants due to generally inadequate LTG activity, rather than absence of specific enzymes, and essential LTG activities are likely independent of protein-protein interactions, as heterologous expression of a non-native LTG rescues growth of a conditionally LTG-null mutant. Lastly, we demonstrate that soluble,

uncrosslinked, endopeptidase-dependent peptidoglycan chains, also detected in the wild-type, are enriched in LTG mutants, and that LTG mutants are hypersusceptible to the production of diverse periplasmic polymers. Collectively, our results suggest that LTGs prevent toxic crowding of the periplasm with synthesis-derived peptidoglycan polymers and contrary to prevailing models, that this autolytic function can be temporally separate from peptidoglycan synthesis.

Introduction

The bacterial cell wall is a nearly universal feature of the bacterial cell envelope. Made primarily of the strong and elastic polymer peptidoglycan (PG), the cell wall preserves bacterial shape while protecting the cell from its high internal turgor pressure and external environmental challenges[1-5]. PG synthesis begins in the cytoplasm with the generation of lipid II, consisting of the disaccharide [N-acetylmuramic acid (MurNAc)-N-acetylglucosamine (GlcNAc)] that is modified with a pentapeptide side stem and attached to the lipid carrier undecaprenol. Lipid II is flipped across the cytoplasmic membrane where the cell wall is assembled in two reactions: First, lipid II is polymerized into longer glycan strands by glycosyltransferases (GTases) followed by crosslinking of the elongating PG strands via their peptide side stems by transpeptidases (TPases)[3,4,6-8]. Ultimately, the combined result of GTase and TPase activities is a covalently closed mesh-like macromolecular network called the PG sacculus.

The strength of the PG sacculus is a double-edged sword. On the one hand, the covalent network provides a mechanical structure strong enough to withstand the high cellular

53 turgor pressure and stresses of a changing environment. On the other hand, it acts as a
54 macromolecular cage that might inhibit cellular expansion and division as well as the
55 insertion of crucial trans-envelope machinery (i.e., flagella and pili).[9-14] Bacteria therefore
56 need to couple new PG synthesis with degradation of bonds within the PG network to
57 simultaneously maintain the integrity of the sacculus while also making space for the
58 insertion of new PG.[11,15,16]
59
60 PG degradation is accomplished by several divergent enzyme classes that are often
61 subsumed under the term "autolysins", i.e., enzymes that cleave various bonds within PG.
62 Endopeptidases (EPs), for example, cleave the peptide crosslinks and are particularly
63 integral to the "space-making" autolytic function that permits sacculus expansion during
64 cell elongation; without EP activity, PG synthesis results in a thicker cell wall or integrity
65 failure and lysis.[17,18] Another major class of autolysins, the lytic transglycosylases (LTGs),
66 cleave the glycosidic linkages between disaccharide subunits within PG strands. Their
67 biochemistry has been exquisitely well-studied and the diversity of their structures and
68 mechanisms of action well characterized.[19-22] Unlike the other autolysins, the primary
69 cleavage mechanism of LTGs is non-hydrolytic. Rather, LTGs perform an intramolecular
70 cyclization of MurNac residues to generate a unique and readily identifiable signature of
71 their activity, anhydro-MurNAc (anhMurNAc).[20,23,24] Early characterization of PG in the
72 bacterial sacculus suggested that every PG strand terminates in an anhMurNAc cap, long
73 implicating LTGs as potential "terminases" of GTase glycan elongation.[23,25] This was only
74 recently confirmed empirically with the novel discovery and characterization of MltG and
75 its functional analogs. [26-29] *E. coli* MltG associates with active PG synthetic complexes to

76 release new strands from the cytoplasmic membrane (to which they are initially tethered
77 via undecaprenyl pyrophosphate), presumably as they emerge from GTase activity;
78 consequently, MltG is a strong determinant of PG strand length.[26-29] Whether association
79 with active GTases is a conserved characteristic of MltG functional analogues (including
80 some hydrolytic glycosidases[30]) has not been established, so these enzymes may be
81 more broadly referred to as "PG release factors" since their cleavage of membrane-bound
82 PG may not directly influence PG elongation. Other physiological roles assigned to LTGs
83 include local PG editing for insertion of PG-spanning protein complexes[10,12,31] and PG
84 recycling. PG recycling, the re-incorporation of PG breakdown products into the
85 biosynthesis cycle, starts with re-uptake of PG turnover products by the importer AmpG.[32]
86 AmpG specifically imports LTG breakdown products (anhMurNAc-containing fragments)
87 and this process can theoretically be supported by any active LTG that produces
88 monomeric anhydromuropeptides. Despite being well-conserved throughout many
89 bacterial phyla, PG recycling is not an essential process under standard growth
90 conditions.[33] Another underappreciated function of LTGs has emerged through the work
91 of our group and others wherein certain individual or combinatorial LTG mutations,
92 including septal LTG RlpA, results in a daughter cell separation defect.[34-37] Intriguingly,
93 the roles of LTGs in all these functions – PG release from the membrane, PG recycling,
94 insertion of PG-spanning complexes, and daughter cell separation – do not appear to be
95 essential to bacterial growth in the contexts studied to date.
96
97 The apparent non-essentiality of lytic transglycosylase activity would seem contradictory
98 to this enzyme class's broad conservation across bacterial phyla (and chloroplasts) as

99 well as genetic and functional redundancy within many individual species – a trait
100 indicative of an important, conserved function.[27] Yet answering the most general
101 physiological questions about LTGs has been severely encumbered by LTG redundancy
102 as rarely does a single LTG mutation yield a significant, readily investigable phenotype.
103 We recently showed that collectively, LTG activity indeed seems to be essential for growth
104 and division.[36] The actual physiological function for the majority of LTGs, however, and
105 the reason for their collective essentiality, has remained elusive. Here, we sought to
106 comprehensively illuminate physiological roles for LTGs by extensively characterizing
107 mutants of the Gram-negative pathogen *Vibrio cholerae* that are defective for most or all
108 of the species' eight currently annotated LTGs. We find that the vast majority of LTGs is
109 dispensable for growth in laboratory media. Minimal LTG strains are defective for growth
110 in low-salt media and hypersensitive to accumulation of periplasmic sugar polymers.
111 Through analysis of PG turnover products, we show that soluble PG strands accumulate
112 in the wild type and that this is exacerbated in ΔLTG mutants and alleviated by inactivating
113 a major PG endopeptidase. Taken together, our data suggest that lytic transglycosylase
114 activity downstream of PG synthesis mitigates toxic periplasmic accumulation of
115 uncrosslinked, polymeric peptidoglycan turnover products released by endopeptidases.
116

117 # Results

118 ***A single LTG is necessary and sufficient for V. cholerae growth***

119 We recently reported that a Δ6 LTG mutant (*rlpA*$^+$ *mltG*$^+$ Δ*mltA* Δ*mltB* Δ*mltC* Δ*mltD* Δ*mltF*
120 Δ*slt70*) was viable under standard laboratory conditions and exhibited only slight
121 morphological defects, including an increase in cell length[36]. Depletion of RlpA from this

122 background resulted in a lethal chaining defect, suggesting that collectively, some degree
123 of LTG activity is essential for *V. cholerae* growth. Since we were previously unable to
124 delete MltG or observe its depletion from a Δ6 LTG background, we asked whether MltG
125 exhibited a synthetic-lethal relationship with the other LTGs using a quantitative
126 insertion/disruption assay. Briefly, we conjugated a suicide vector targeting *mltG* (or
127 positive or negative control loci) into WT and Δ6 LTG and quantified viable recombinants.
128 Surprisingly, the WT and Δ6 LTG strains both tolerated inactivation of *mltG* by the suicide
129 vector so long as essential DNA synthesis genes downstream of *mltG* were expressed *in*
130 *trans* to ameliorate polar effects of *mltG* disruption (Figure 1A, Figure 1 – Figure
131 supplement 1AB). The resulting Δ6 LTG *mltG::kan* mutant was viable in LB but failed to
132 grow in low-salt LB (LB without added NaCl, hereafter designated LB0N) (Figure 1 –
133 Figure supplement 1C), which could explain why previous attempts to inactivate *mltG* in
134 this background using SacB-based allelic exchange (requiring selection on
135 LB0N+sucrose) were unsuccessful[36]. Consistent with these data, we were then able to
136 generate a clean, viable Δ7 LTG mutant (*rlpA*$^{+}$ *mltG::stop* Δ*mltABCDF* Δ*slt70*) using a
137 MqsR toxin-based allelic exchange system.[38] The Δ7 mutant sacculus contained only a
138 tenth of the AnhMurNAc residues observed in the wild type sacculus (Figure 1 – Figure
139 supplement 1D, Supplemental File 1), suggesting that there is significantly reduced LTG
140 activity in the Δ7 LTG mutant. Additionally, by placing the native copy of *rlpA* under an
141 arabinose-inducible promoter, we were able to conditionally deplete RlpA by growing
142 these strains in the absence of arabinose to observe the effects of LTG insufficiency
143 (Figure 1B, Figure 1 – Figure supplement 2). Compared to Δ6 LTG[36], RlpA depletion was

144 more severe in the Δ7 background, both by morphology and plating efficiency, consistent
145 with Δ7 exhibiting more limited LTG activity than Δ6.
146
147 Importantly, we confirmed that growth of Δ7 LTG depended on RlpA LTG activity, as
148 RlpA^{D145A}, a predicted active site mutant[35] (Figure 1 – Figure supplement 3AD) was
149 unable to promote growth despite being stably produced (Figure 1 – Figure supplement
150 4) and maintaining septal recruitment as indicated by the septal localization of an
151 RlpA^{D145A}-mCherry fusion (Figure 1C, Figure 1 – Figure supplement 4). Conversely, we
152 found that a truncated RlpA mutant lacking the conserved SPOR domain (which is
153 essential for septal localization in *P. aeruginosa*[35]) no longer localized to the division
154 septum in *V. cholerae* as an mCherry fusion (Figure 1 – Figure supplement 3C) yet still
155 fully complemented native RlpA depletion in both Δ6 and Δ7 (Figure 1C, Figure 1 – Figure
156 supplement 4), suggesting that RlpA LTG activity, but not septal localization, are essential
157 in these backgrounds. Taken together, these results demonstrate that at least during
158 growth in standard laboratory conditions, *V. cholerae* requires at least one active LTG of
159 the 8 currently annotated in its genome.
160
161 ***Only a subset of LTGs can independently fulfill all essential LTG functions***
162 Since RlpA LTG activity, but not septal localization, was essential for Δ6 and Δ7 growth,
163 we asked whether growth required specialized LTG function, or just PG cleavage function
164 in general. To test this, we assessed the ability of other LTGs to complement Δ6 and Δ7
165 (Figure 1C, Figure 1 – Figure supplement 4). Only two native LTGs, MltD and Slt70, could
166 fully (MltD) or partially (Slt70) substitute for RlpA in the Δ7 LTG background,

167 demonstrating that RlpA, MltD, and (to a lesser degree) Slt70 are the only *V. cholerae*
168 LTGs capable of fulfilling all required LTG roles. Additional LTGs, MltA, MltB, and MltC,
169 were able to rescue RlpA depletion in the Δ6 LTG background (where MltG is present),
170 but not the Δ7 LTG background (where MltG is absent). These observations suggest that
171 LTGs perform at least two separable essential functions for viability, where MltG can
172 perform one function but requires MltA, MltB, or MltC to perform another, and vice versa,
173 as none of these LTGs are independently capable of supporting growth. Intriguingly, the
174 *E. coli* LTG MltE, for which *V. cholerae* has no known homologue, was also capable of
175 fully supporting *V. cholerae* growth as the sole functioning LTG, suggesting that LTG
176 essential functions may not depend on specific protein-protein interactions. Collectively,
177 these data suggest that LTGs are partially redundant; but some LTGs also exhibit varying
178 degrees of functional specificity.
179
180 ***LTGs are required during vegetative growth***
181 We were surprised that our strains lacking major LTG activity (even Δ7) were viable. We
182 thus sought to characterize growth and morphology of these backgrounds in more detail.
183 While the Δ6 and Δ7 mutants grew at wild-type growth rates in LB medium when cultures
184 were started from a 100-fold dilution of saturated overnight cultures, we noticed a dilution-
185 dependent exacerbation of growth and morphology defects (Figure 2, Figure 2 – Figure
186 supplement 1, Figure 2 – Figure supplement 2). When Δ7 LTG cultures were highly diluted
187 from overnight cultures to increase the number of generations spent in exponential
188 growth, we started to observe a marked growth defect (Figure 2AB, Figure 2 – Figure
189 supplement 2A). Conversely, the *mltG::stop* single mutant and Δ6 LTG mutant grew at

190 wild-type growth rates independent of initial dilution factor (Figure 2B, Figure 2 – Figure
191 supplement 2A). These data suggest an essential or near-essential role for MltG during
192 sustained exponential growth, albeit only when other LTGs are also inactivated. We also
193 observed diverse aberrant morphologies within the LTG-deficient mutants (but not a
194 Δ*mltG*::stop single mutant) under these conditions (Figure 2C, Figure 2 – Figure
195 supplement 1). Interestingly, despite lacking most members of an entire class of PG
196 enzymes, Δ6 and Δ7 only exhibited only mild defects in length and width homeostasis
197 (Figure 2DE, Figure 2 – Figure supplement 2), which were only dilution-factor dependent
198 for cell length (suggesting a cumulative division defect). When we followed a time-course
199 after back-dilution from stationary phase, we observed morphological defects
200 accumulating in exponential phase and then largely disappearing in stationary phase
201 (Figure 2 – Figure supplement 3) in both Δ6 and Δ7. Collectively, these observations
202 suggest that LTG-deficient mutants suffer from cumulative damage during exponential
203 growth, which is partially alleviated in stationary phase.
204
205 ***LTG activity is required for survival in hypo-osmotic conditions***
206 Our results detailed above suggested that the majority of LTGs are dispensable for
207 growth, catalyzing renewed interest in the question of what their physiological roles are.
208 To dissect potential roles for LTGs in cell envelope integrity maintenance, we subjected
209 the Δ6 and Δ7 mutants to growth in low osmolarity medium. Similar to the morphology
210 and growth defects in LB, both mutants were sensitive to low salt conditions in a dilution-
211 dependent manner (Figure 3A, Figure 3 – Figure supplement 1). Interestingly, the Δ7 LTG
212 mutant grew at wild-type rate during the initial growth period before a rapid decrease in

213 OD_{600}, indicative of lysis, suggesting that it is not the initial shock of changing osmotic
214 conditions that kills this mutant, but rather some cumulative damage during growth in low-
215 salt conditions (Figure 3A, Figure 3 – Figure supplement 1A). Importantly, this rules out
216 a simple cell envelope defect as a cause of LTG-deficient mutant osmo-sensitivity. We
217 then sought to dissect the contributions of individual LTGs to salt sensitivity. Other than
218 RlpA, which has an established role in LB0N growth[35,36] and is still present in the Δ6 and
219 Δ7 mutants, no other single LTG mutant exhibited a strong growth defect in LB0N (Figure
220 3 – Figure supplement 2A), all further suggesting that this defect is an accumulative
221 function of collective LTG insufficiency. Several LTGs (MltA, MltB, Slt70, and EcMltE)
222 were able to rescue Δ6 LTG growth in LB0N at higher dilutions (Figure 3 – Figure
223 supplement 2C), but none could rescue Δ7 growth in LB0N except MltG, which only
224 partially restored growth to Δ6 mutant levels (Figure 3 – Figure supplement 2D). This
225 suggests that no single LTG can fully support growth in LB0N, and that MltG, despite not
226 exhibiting a defect as a single mutant, is particularly important in this environment when
227 other LTGs are inactivated. Intriguingly, overexpression of *mltF* was toxic for both the Δ6
228 (LB0N only) and the Δ7 mutant (LB) (Figure 3 – Figure supplement 2BCD), preventing us
229 from assessing its potential for LTG-deficient mutant complementation.
230
231 ***LTG mutants are hypersensitive to accumulation of periplasmic polysaccharides***
232 To determine the reason for ΔLTG defects in low salt media, we took advantage of the
233 spontaneous appearance of suppressors arising during Δ6 LTG growth in LB0N. (Figure
234 3B, Figure 3 – Figure supplement 1B). Whole genome sequencing of three stable
235 suppressors identified three unique mutations: a deletion in *ptsH* (*vc0966*), a frameshift

236 mutation in *opgH* (*vc1287*), and a deletion mutation affecting both *opgH* and a
237 downstream gene (*vc1286*) (Figure 3C). *ptsH* encodes HPr, a key regulator of sugar
238 import via the phosphoenolpyruvate-carbohydrate phosphotransferase system (PTS).[39]
239 OpgH is critical to the synthesis of periplasmic glucans (OPGs), which accumulate under
240 conditions of low osmolarity and have been implicated in a variety of cell functions,
241 including steady-state maintenance of osmolarity in the periplasm.[40] We were particularly
242 intrigued by the role of periplasmic glucans and validated restoration of Δ6 LTG LB0N
243 growth using clean deletion mutants. Inactivation of *opgH* completely restored wild-type
244 growth of the Δ6 LTG mutant in LB0N, independent of initial dilution factor (Figure 3D,
245 Figure 3 – Figure supplement 1E). In contrast, inactivation of *opgH* was only able to
246 restore growth of the Δ7 LTG mutant in LB0N from a 10^{-2} inoculum (Figure 3D, Figure 3
247 – Figure supplement 1E), but not from greater dilutions, nor from a 10^{-5} inoculum in LB
248 (Figure 3 – Figure supplement 1CD), indicating that the Δ7 LTG mutant has additional
249 exponential growth-dependent defects unique from the Δ6 LTG mutant. Interestingly,
250 OpgH orthologues in *E. coli* and *Y. pseudotuberculosis* have also been ascribed a
251 moonlighting function, tying carbon availability with cell length by inhibiting FtsZ
252 filamentation when UDP-glucose levels are high in the cell[41,42]. The elongated cell
253 phenotype of the Δ6 LTG and Δ7 LTG mutants could in principle be indicative of a similar
254 activity by *V. cholerae* OpgH; however, deleting *opgH* from the Δ6 LTG mutant did not
255 restore wild-type cell length in Δ6 (Figure 3 – Figure supplement 3A). Additionally,
256 alignment of *V. cholerae* OpgH with *E. coli* and *Y. pseudotuberculosis* suggests that it
257 lacks much of the N-terminal domain that was shown to interact with FtsZ in *E. coli* (Figure
258 3 – Figure supplement 3B).[41]

259

260 We consequently considered a model where accumulation of periplasmic glucans is
261 detrimental to ΔLTG mutants, e.g., via periplasmic crowding or an increase in periplasmic
262 osmolarity. To test this model, we used an unrelated system to increase periplasmic
263 crowding. The *B. subtilis sacB* gene product, which is secreted and functions
264 extracellularly[43], isomerizes and polymerizes sucrose monomers into levan molecules up
265 to several kD[44], molecules much too large to escape the gram-negative periplasm through
266 outer membrane porins. This is often exploited in allelic exchange methods for mutant
267 generation as a means of counterselection,[45-47] where, for example, WT *V. cholerae* is
268 sensitive to *sacB* expression in LB0N+sucrose. We hypothesized that the ΔLTG mutants
269 might be hypersensitive to periplasmic levan synthesis even in standard LB salt
270 conditions (1% W/V). To test this, we engineered strains overexpressing *sacB*. Consistent
271 with the use of *sacB* as a counterselection method under low salt conditions, the wild type
272 is sensitive to *sacB* induction on LB0N (Figure 3 – Figure supplement 4), but not LB. In
273 contrast, we observed a *sacB*-dependent plating defect on sucrose in the Δ6 and Δ7 LTG
274 mutant on LB (Figure 3E, Figure 3 – Figure supplement 4). Interestingly, the *mltG::stop*
275 mutant also exhibited hypersensitivity to SacB activity (Figure 3E, Figure 3 – Figure
276 supplement 4), suggesting that accumulating MltG substrate is a particularly strong direct
277 or indirect contributor to this phenotype. Collectively, our data suggest that ΔLTG mutants
278 suffer from either hyperosmotic stress or excessive molecular crowding in the periplasm,
279 which can be exacerbated through the induction of long-chain polysaccharides.

280

281 ***PG transglycosylase activity causes Δ6 LTG mutant periplasmic stress***

282 Based on our model that accumulation of polysaccharides in the periplasm is toxic, we
283 predicted that accumulation of uncrosslinked PG strands caused by uninterrupted GT
284 activity during TP inhibition, e.g. by β-lactams[48] (a process termed "futile cycling" when
285 coupled with LTG-mediated degradation[48]) should exacerbate LTG-deficient mutant
286 sickness, and this has indeed been shown with Slt70 in *E. coli*[48]. To test this hypothesis,
287 we assessed susceptibility of ΔLTG mutants to cell wall-acting antibiotics with varying
288 ability to induce futile cycling. In a disk diffusion assay, the Δ6 and Δ7 LTG mutants were
289 hypersensitive to inducers of futile cycling, i.e., general PBP inhibition by Penicillin G as
290 well as to inhibition of specific PBPs including PBP3 (aztreonam), PBP2 (mecillinam), and
291 PBP1b (cefsulodin) (Figure 4A). Conversely, both the Δ6 and the Δ7 mutant exhibited
292 wild-type sensitivity to moenomycin and fosfomycin, both of which inhibit cell wall
293 synthesis without inducing futile cycling. Thus, β-lactam sensitivity of LTG-deficient
294 mutants is not necessarily tied to simple inhibition of cell wall synthesis, but potentially
295 also to periplasmic crowding due to the accumulation of uncrosslinked PG strands.
296 Curiously, the Δ7 LTG mutant was hypersensitive to MreB inhibition by MP265. This
297 suggests that in the absence of other LTGs, MltG contributes to survival upon Rod system
298 insufficiency through an unknown mechanism.
299
300 To further dissect PG strand accumulation under these conditions, we visualized PG
301 synthesis and turnover during antibiotic treatment using the cell wall label BADA.[49,50] The
302 Δ6 and Δ7 LTG mutants were all readily labeled when grown with BADA (Figure 4 – Figure
303 supplement 1, Figure 4 – Figure supplement 2) prior to antibiotic addition. Upon treatment
304 with cell wall-targeting antibiotics, WT *V. cholerae* degrades its structural, rod-shaped

305 sacculus to ultimately yield stable, cell wall-deficient spheroplasts.[51,52] After up to 3 hours
306 of treatment with Penicillin G (100μg ml^{-1}, 20xMIC) and continued incubation with BADA,
307 the Δ6 and Δ7 LTG mutant spheroplasts accumulated strong periplasmic BADA signal
308 compared to the wild-type spheroplasts in which cell wall material is presumably
309 completely degraded and removed from the periplasm (Figure 4B, Figure 4 – Figure
310 supplement 1). Meanwhile, in the Δ6 and Δ7 LTG mutants, uncrosslinked PG likely
311 accumulates due to aberrant GT activity. Alternatively, degraded PG from the sacculus
312 may be sufficiently retained in the periplasm to be additionally labeled with BADA by L,
313 D-transpeptidases[53] in the Δ6 and Δ7 LTG but not in the WT. However, inhibition of cell
314 wall synthesis upstream of GT activity using fosfomycin (500μg ml^{-1}) (which is expected
315 to result in sacculus degradation without induction of futile cycling) did not result in
316 pronounced BADA accumulation in the periplasm, suggesting that the increasing BADA
317 signal observed during penicillin treatment does not solely reflect retention of labeled
318 debris from the degraded sacculus, but indeed is the result of ongoing cell wall synthesis
319 (Figure 4B, Figure 4 – Figure supplement 2). The diffuse nature of the BADA signal
320 additionally suggests that the PG in the Δ6 and Δ7 spheroplasts is solubilized debris
321 trapped in the periplasm, as opposed a thin, intact layer of peripheral PG. At earlier
322 stages of penicillin treatment, it also appeared that the Δ6 and Δ7 LTG mutants were
323 slower to degrade their rod-shaped poles (Figure 4 – Figure supplement 1).
324

325 ***PG recycling is not required during periplasmic stress***

326 The roles for LTGs in PG recycling are well characterized. LTGs are required to digest
327 longer glycan strands down to single disaccharide subunits which can be imported into

328 the cytoplasm via AmpG, a permease that selectively recognizes the anhMurNAc residue
329 generated by LTG activity. Mutants lacking AmpG have been demonstrated to
330 accumulate extracellular monomeric disaccharide LTG-turnover products[54]. We therefore
331 asked whether a lack of recycling could account for some of our key phenotypes.
332 However, an Δ*ampG* mutant exhibited wild-type behavior for growth in LB0N, sacB
333 overexpression, beta-lactam resistance, and BADA staining after PenG exposure (Figure
334 4 – Figure supplement 3), demonstrating that lack of PG recycling does not promote the
335 LTG-deficient phenotypes observed here.
336

337 ***LTG insufficiency results in periplasmic PG strand accumulation***

338 Why are LTG mutants sensitive to periplasmic accumulation of polymers? Accumulating
339 PG debris released during PG synthesis could, in principle, increase periplasmic
340 osmolarity and/or crowding, explaining defects associated with low salt conditions and
341 periplasmic polysaccharide accumulation. We therefore sought to quantify soluble,
342 periplasmic PG debris within crude cell lysates (excluding PG released into the growth
343 medium). Canonical PG architecture analysis relies on SDS-boiled sacculi isolated by
344 ultra-centrifugation, which permits sacculus characterization (Figure 1 – Figure
345 supplement 1D, Supplemental File 1), but ignores solubilized, uncrosslinked (freely-
346 diffusing) PG fragments associated with PG turnover processes such as those potentially
347 mediated by LTGs. We thus analyzed fragments that remained soluble after
348 sedimentation of purified sacculi, i.e., PG material that freely accumulates within the
349 periplasm (or inside the cell) but is not attached to the cell wall. Since entire periplasmic
350 PG strands cannot be easily resolved using subsequent LC-MS analysis, we also

351 digested the soluble PG fraction with muramidase (to generate smaller monomers
352 suitable for LC-MS detection) and then compared muramidase-treated vs. untreated
353 traces to determine soluble PG architecture (Figure 5A). We first analyzed soluble
354 products of LTG activity (Figure 5BC, Supplemental File 2). AnhMurNAc-tetrapeptide
355 (M4N) was abundant in the wild type during exponential phase, and predictably, M4N was
356 significantly depleted in the Δ7 LTG soluble muropeptide profile. Surprisingly, M4N was
357 enriched in the *mltG::kan* and Δ6 LTG mutants, suggesting that the absence of some
358 LTGs might cause upregulated activity of others.
359
360 Importantly, MurNAc-tetrapeptide species without anhMurNAc (M4) were detectable in
361 the WT during exponential phase, and significantly enriched in the Δ6/Δ7 LTG mutants
362 (Figure 5D, Supplemental File 2). By comparing the muramidase-treated vs. untreated
363 samples, we can infer the native state of these M4 and M4N (Figure 5ABD), i.e.,
364 determine whether these species occur predominantly as monomers or as parts of PG
365 polymers *in vivo*. Both species were significantly depleted in the muramidase-untreated
366 samples, suggesting that *in vivo*, they are part of polymeric, uncrosslinked peptidoglycan
367 strands. It is important to note that M4 monomers are not intermediates of cell wall
368 synthesis (which proceeds from a tripeptide directly to pentapeptide due to addition of
369 preformed D-Ala-D-Ala dipeptide).[55] This, in conjunction with a strong muramidase-
370 treatment-dependence of the abundance of M4 excludes a cytoplasmic origin of this
371 species. It is also interesting to note that, unlike the WT, *mltG::kan*, and even Δ6 LTG
372 mutant, the Δ7 LTG appears to have a disproportionately large pool of polymeric M4
373 species (muramidase-dependent) compared to M4N species, suggesting that either the

374 soluble PG strands in the Δ7 LTG mutant are extremely long, or perhaps do not
375 ubiquitously terminate in anhMurNAc residues. The abundance of soluble PG strands
376 decreased in stationary phase (Figure 5CE, Supplemental File 2), which suggests that in
377 the LTG-deficient mutants, these strands are somehow cleared by RlpA, an unrecognized
378 LTG, or a cryptic PG hydrolase. Reduction of these uncrosslinked strands in stationary
379 phase is consistent with the alleviation of morphology defects observed as cells exit
380 exponential growth (Figure 2 – Figure supplement 3).
381
382 We next asked how these polymeric, uncrosslinked PG strands might be generated.
383 Since endopeptidases have been suggested to be essential for sacculus expansion
384 during cell elongation, we hypothesized that these soluble strands may reflect
385 endopeptidase activity, which would imply that EPs do not simply relax PG crosslinking
386 (as commonly assumed), but also might excise entire strands that accumulate - at least
387 transiently - in the periplasm. To test this hypothesis, we depleted the major
388 housekeeping EP ShyA[56] from a Δ6 LTG mutant, and found that the most abundant
389 monomer species, M4, was reduced in a ShyA-dependent manner in both the WT and
390 Δ6 LTG mutant (Figure 5F, Supplemental File 3). This strongly suggests that ShyA
391 produces the majority of the uncrosslinked strands in the periplasm. Curiously, depletion
392 of ShyA in the Δ6 LTG background resulted in large, irregular cells (Figure 5 – Figure
393 supplement 1), suggesting a cell envelope defect upon EP insufficiency. Additionally,
394 ShyA was required for Δ6 LTG mutant colony formation on LB plates, but Δ6 LTG liquid
395 cultures depleted for ShyA remained viable and could be rescued on plates restoring
396 *shyA* expression (Figure 5 – Figure supplement 1). Altogether, the data suggest that EPs

397 excise entire PG strands that accumulate in the periplasm until they are later cleared by
398 LTGs.
399

400 ## Discussion

401 Despite decades of work and a renewed research focus in the last few years, we still lack
402 a fundamental understanding of how bacteria harness both PG synthesis and constant
403 degradation to build and maintain an essential and dynamic wall structure that is able to
404 withstand a high internal turgor pressure. Even the basic physiological function of many
405 cell wall cleavage enzymes ("autolysins") remains unknown. The exact contributions of
406 LTGs to cell growth, for example, have remained elusive, mainly due to the high level of
407 apparent redundancy of these enzymes, which hampered classical genotype-phenotype
408 association analyses. While circumstantial evidence abounds, no collective physiological
409 characterization of essential LTG function has been conducted in any organism, and even
410 cases of demonstrated synthetic lethal relationships are rare and rely on indirect evidence
411 (inability to delete LTG genes).[34,57,58] The *V. cholerae* Δ6 and Δ7 LTG mutants described
412 here provide a vital platform for exploring both the collective and individual contributions
413 of lytic transglycosylases to bacterial viability.
414

415 ***Conserved LTGs are not functionally equivalent***

416 In this study we confirm that LTG enzymatic activity is essential for growth and division.
417 We further demonstrate that some functional redundancy exists in *V. cholerae* between
418 diverse LTG families, as has been observed in other bacteria [12,20,59]. Members of LTG
419 families 1A (Slt70), 1D (MltD) and 6A (RlpA) can support growth independent of all other

420 natively encoded LTGs from families 1B, 1E, 2A, 3A, and 5A. Certain *V. cholerae* LTGs
421 additionally exhibit complementary genetic relationships in the absence of all other LTGs,
422 implying there are at least two essential roles for LTGs. For example, while neither MltG,
423 MltA, MltB, nor MltC can support growth on their own, strains expressing the MltG+MltA,
424 MltG+MltB, or MltG+MltC pairs are each viable. Surprisingly, and importantly, essential
425 LTG activities may not require conserved protein-protein interactions as suggested by the
426 viability of a *V. cholerae* mutant expressing non-native *E. coli* MltE as its sole LTG.
427 Scheurwater and Clarke unsuccessfully but informatively attempted to inactivate *mltF* in
428 an *E. coli* Δ6 LTG (Δ*mltABCDE* Δ*slt70*), suggesting that the essentiality of LTG activity is
429 conserved between *E. coli* and *V. cholerae,* and that MltF and MltG may not be
430 functionally redundant in *E. coli*.[58] In contrast, *mltF* inactivation is not synthetically lethal
431 with Δ*mltABCD* Δ*slt70* in *V. cholerae*. In fact, restoring MltF expression in the Δ6 and Δ7
432 LTG background is toxic, indicating that *V. cholerae* and *E. coli* exhibit different genetic
433 relationships between homologs of the same LTGs. This is perhaps most strongly
434 exemplified by the conservation of RlpA in both species, where *E. coli* RlpA has no
435 detectable LTG activity[35], yet *V. cholerae* RlpA can perform essential functions as the
436 sole LTG. Recently, the hydrolytic enzyme DigH in *E. coli* was shown to be functionally
437 similar to LTGs by contributing to the resolution of septal PG during daughter cell
438 separation[60]. The activity of DigH (of which *V. cholerae* does not possess a strong
439 homolog) may explain why *E. coli* does not appear to require RlpA LTG activity; this LTG-
440 like physiological role for a hydrolytic enzyme also suggests that we may need to look
441 beyond LTGs to fully address the roles for glycosidic bond cleavage within PG. Another
442 recent example of glycosidases serving as functional analogues includes MpgA from *S.*

443 *aureus* which shares enough homology with MltG to be identified bioinformatically as a
444 YceG-family LTG but harbors a single active site mutation to impart a muramidase
445 mechanism of PG cleavage.[30]
446
447 The functional redundancy of LTGs is also likely the root of an apparent paradox. Release
448 of new PG strands from undecaprenyl pyrophosphate should be an essential function, as
449 anchoring of PG to the inner membrane is toxic[61] and is likely necessary for lipid carrier
450 recycling. Yet MltG, the highly conserved "PG terminase," or more generally, "PG release
451 factor," that associates with PG synthetic complexes to release new strands, is not
452 essential. MltG can be inactivated in wild type *V. cholerae* (and *E. coli*) without significant
453 consequence, but our Δ7 LTG (*mltG*-null) mutant lost viability upon sustained growth in
454 exponential phase in LB. It is therefore likely that other LTGs can partially complement
455 for PG release activity. The dilution-dependent Δ7 LTG growth defect further suggests
456 that either RlpA has at least partial PG release activity and/or that during brief growth in
457 exponential phase, PG release activity is non-essential. MltG essentiality (or near-
458 essentiality) can thus perhaps only be appreciated in a multiple LTG background under
459 conditions where PG release activity is expected to be most important. This is also
460 evidenced by the increased sensitivity of the Δ7 LTG mutant to hypo-osmotic conditions
461 that cannot be rescued via the same mechanisms that rescue Δ6 LTG mutant, i.e.,
462 inactivation of OPG synthesis, as well as hypersensitivity to MreB-inhibitor MP265. All of
463 these defects point to a unique, MltG-dependent, conditionally essential LTG function.
464 While this study has focused on clearance of soluble PG debris, an activity that would
465 perhaps only be critical in organisms with a membrane-confined periplasmic space, PG

466 release factors analogous in function to MltG are broadly conserved even in Gram
467 positive organisms, additionally demonstrating a necessity for further investigation into
468 the role of PG release in bacterial cell wall homeostasis.
469
470 ***LTGs manage the periplasmic environment***
471 By analyses of soluble PG, we discovered that even wild-type *V. cholerae* accumulates
472 loose strands of uncrosslinked PG of periplasmic origin (detected as muramidase-
473 dependent, soluble M4 products) and that production of these strands is dependent on
474 the EP ShyA. PG strands appear to accumulate to detrimental levels in the Δ6 and Δ7
475 mutants and we thus propose that processing soluble PG is a major collective function of
476 LTGs. PG strand accumulation induces hypersensitivity to other polymeric sugars in the
477 periplasm, such as OPGs, SacB-generated levans and β-lactam-induced futile cycling
478 products. Since these hypersensitivities are not shared by a Δ*ampG* mutant, previously
479 demonstrated to accumulate small PG monomers, this polysaccharide toxicity may arise
480 from the fact that these large polymers (PG, OPGs, or levans) cannot diffuse out through
481 OM porins, accumulating in a growth and/or substrate-dependent manner. This would
482 inappropriately increase the osmolarity and/or cause excessive crowding[5] of the
483 periplasm to interfere with normal growth-related processes, as exemplified by the mild
484 division defect of the *V. cholerae* LTG-deficient mutants.
485
486 While periplasmic crowding can clearly occur in Gram-negative bacteria due to their
487 diffusion-limiting OM, it is intriguing to consider implications for Gram-positives, where
488 LTGs are likewise conserved, and the cell wall may not provide a meaningful diffusion

489 barrier to long PG strands. We propose three possible (and testable) scenarios for the
490 role of LTGs in Gram-positive bacteria. For example, only PG release activity might be
491 essential in Gram-positives. It is also conceivable that LTGs are non-essential in Gram-
492 positive bacteria. Lastly, "periplasmic" crowding may in fact be detrimental in Gram-
493 positive bacteria: *B. subtilis* PG, for example, is very long chained and it is conceivable
494 that PG may constitute a reasonable diffusion barrier against such long strands.
495
496 ***Broader implications for LTGs in PG dynamics***
497 Our data suggest that the most important roles for LTGs may not include "making space"
498 for new PG insertion, as has been assumed for fundamental models of PG synthesis.
499 More likely, LTGs clear the periplasm of most PG debris generated by endopeptidases
500 during normal growth by facilitating either recycling or release of small fragments into the
501 environment (Figure 6). As such, this collectively essential function of LTGs may not be
502 tied to a direct influence on PG synthesis. Importantly, uncrosslinked strands are not a
503 deviant feature unique to the LTG-deficient mutants nor β-lactam treatment (though they
504 become more apparent under these conditions), as they were also detectable in the wild
505 type during normal growth. Detection of EP-dependent, uncrosslinked PG strands
506 suggests that EP activity might be temporally separated from LTG-mediated turnover of
507 those PG strands. This is seemingly contrary to pervasive models proposing a
508 synchronized synthetic/autolytic complex that digests old PG while simultaneously
509 building new PG. If such a complex exists, we propose that LTGs collectively maintain an
510 important role complementary to it, but not inevitably as part it.
511

512 Lastly, while high accumulation of PG strands is toxic, maintaining a small pool of
513 uncrosslinked PG material may actually serve a beneficial purpose to cells under some
514 conditions; bacteria might thus have an adaptive reason for avoiding tightly coordinating
515 LTG activity with synthesis. Inactivation of *sltY* in *E. coli,* for example, can promote β-
516 lactam resistance by upregulating L,D-crosslinking activity of L,D-transpeptidase LdtD
517 (YcbB), presumably due to the increased presence of uncrosslinked glycan strands under
518 these conditions.[62] It is possible that one function of L,D-TPs is to patch holes in the
519 sacculus via readily available soluble PG strands, constituting an innate "bike tire repair
520 kit" for the bacterial cell wall. Future studies of this LTG-mediated turnover of
521 uncrosslinked PG could be critical for understanding PG repair mechanisms, as well as
522 general periplasmic homeostasis, both of which have been historically elusive topics.
523

524 ## Materials and Methods

Key Resources Table				
Reagent type (species) or resource	**Designation**	**Source or reference**	**Identifiers**	**Additional information**
gene (*V. cholerae*)	*mltA*	UniProtKB	*vc_2312*	
gene (*V. cholerae*)	*mltB*	UniProtKB	*vc_1956*	
gene (*V. cholerae*)	*mltC*	UniProtKB	*vc_0450*	
gene (*V. cholerae*)	*mltD*	UniProtKB	*vc_2237*	

gene (*V. cholerae*)	*mltF*	UniProtKB	*vc_0866*	
gene (*V. cholerae*)	*mltG*	UniProtKB	*vc_2017*	
gene (*V. cholerae*)	*rlpA*	UniProtKB	*vc_0948*	
gene (*V. cholerae*)	*slt70*	UniProtKB	*vc_0700*	
gene (*V. cholerae*)	*shyA*	UniProtKB	*vc_a0079*	
gene (*V. cholerae*)	*opgH*	UniProtKB	*vc_1287*	
gene (*V. cholerae*)	*ampG*	UniProtKB	*vc_2300*	
gene (*V. cholerae*)	*lacZ*	Kegg2 Gene DB	*vc_2338*	
gene (*E. coli*)	*EcrlpA*	UniProtKB	*b0633*	
gene (*E. coli*)	*EcmltE*	UniProtKB	*b1193*	
gene (*P. aeruginosa*)	*ParlpA*	UniProtKB	*pa4000*	
gene (*B. subtilis*)	*sacB*	UniProtKB	*bsu34450*	

Strain, strain background (*V. cholerae*)	El Tor N16961; wild-type	PMID: 243277		
Recombinant DNA reagent	Δ*mltABCDF* Δ*slt70;* Δ6 LTG	PMID: 31286580		
Recombinant DNA reagent	Δ*mltABCDF* Δ*slt70 mltG::stop;* Δ7 LTG	This Study		See Supplemental File 4; Request from Doerr lab
Recombinant DNA reagent	*mltG::stop*	This Study		See Supplemental File 4; Request from Doerr Lab
Recombinant DNA reagent	pCVD442	PMID: 15109831		
Recombinant DNA reagent	pTOX5	PMID: 31201277	Addgene #127450	
Recombinant DNA reagent	pAM224; pGP704-kanR	PMID: 2836362		
Recombinant DNA reagent	pAM299	PMID: 25631756		
Recombinant DNA reagent	pJL1	PMID: 24348240		
Antibody	anti-mCherry (rabbit polyclonal)	GeneTex	GTX59788	(1:5,000)
Antibody	Goat anti-rabbit IRDye 800CW secondary	Li-cor	926-32211	(1:16,000)

Antibody	anti-RpoA (mouse monoclonal)	BioLegend	663104	(1:10,000)
Antibody	Goat anti-mouse IRDye 800CW secondary	Li-cor	926-32210	(1:16,000)
Chemical compound, drug	Penicillin G potassium salt	Fisher Scientific	CAS: 113-98-4	
Chemical compound, drug	Aztreonam	Fisher Scientific	CAS: 78110-38-0	
Chemical compound, drug	Mecillinam	Sigma Aldrich	CAS: 32887-01-7	
Chemical compound, drug	Cefsulodin sodium salt hydrate	TCI Chemicals	CAS: 1426397-23-0	
Chemical compound, drug	S-(4-Chlorobenzyl) Isothiouronium chloride (MP265)	Chem Impex International	CAS: 544-47-8	
Chemical compound, drug	Phosphomycin disodium salt (Fosfomycin)	Sigma Aldrich	CAS: 26016-99-9	
Software, algorithm	FIJI	PMID: 22743772		
Software, algorithm	MicrobeJ	PMID: 27572972		
Software, algorithm	Oufti	PMID: 26538279		
Other	BADA	PMID: 28989665		

527 ***Bacterial strains and growth conditions***

528 *V. cholerae* strains in this study are derivatives of *V. cholerae* WT El Tor strain N16961
529 [63]. Construction of plasmids and mutant *V. cholerae* strains is described in the next
530 section along with a table of strains and plasmids used in this work (Supplemental File
531 4).

532

533 Strains were grown at 30°C or 37°C in Luria-Bertani (LB-Miller, Fisher Bioreagents#
534 BP97235) with or without 1% NaCl, 1% sucrose, or 10% sucrose, or in M9 minimal media
535 + 0.4% glucose (Cold Spring Harbor Protocols) where indicated in the figure legends.
536 Growth media were supplemented with kanamycin (50 µg ml^{-1}), ampicillin (25 µg ml^{-1}), or
537 chloramphenicol (5 µg ml^{-1}) in plates and overnight cultures when needed to maintain
538 plasmids or chromosomal integration of suicide vectors. Genes under P_{ara} and P_{tac}
539 regulation were induced with 0.4% L-arabinose or 200 µM isopropyl-β-D-1-
540 thiolgalactopyranoside (IPTG), respectively.

541

542 ***Construction of plasmids and strains***

543 A summary of all strains, plasmids, and primers used in this study can be found in Tables
544 S9-S11. *E. coli* DH5α λ*pir* was used for general cloning, while *E. coli* SM10 or MFD λ*pir*
545 were used for conjugation into *V. cholerae*[64]. Plasmids were constructed using Gibson
546 assembly[65] with the exception of plasmids expressing *rlpA*Δ*SPOR* or *rlpA*^{D145A}, which
547 were generated by site directed mutagenesis of the parent wild-type sequence *rlpA*
548 plasmids. All Illumina whole genome sequencing and variant calling for Δ6 LTG and Δ7

549 LTG strain verification or suppressor identification was performed by the Microbial
550 Genome Sequencing Center (MiGS, Pittsburg, PA, USA).
551
552 Most chromosomal in-frame deletions (or premature stop codon mutants) were generated
553 using the pCVD442 *ampR/sacB* allelic exchange system[66]. 500bp regions flanking the
554 gene to be deleted were amplified from N16961 genomic DNA by PCR, cloned into
555 suicide vector pCVD442, and conjugated into *V. cholerae*. Conjugation was performed
556 by mixing and pelleting equal volumes of recipient *V. cholerae* and SM10 or MFD λ*pir*
557 donor LB overnight cultures, spotting the mixed pellet onto LB (+600 μM diaminopimelic
558 acid [DAP] for MFD λ*pir*) followed by incubation at 37°C for 3 hrs. The first round of
559 selection was performed on LB + streptomycin (200 μg ml^{-1}) + ampicillin (100 μg ml^{-1}) at
560 30°C followed by counterselection on salt-free LB + 10% sucrose + streptomycin at room
561 temperature. Inducers for conditionally essential genes were included in all media during
562 conjugation and selection. Addition of 0.2% glucose was required for maintenance in *E.*
563 *coli* of plasmids expressing *Vc mltB*. Deletions were verified by PCR.
564
565 Introduction of a premature stop codon to *mltG* at its native locus to yield Δ7 LTG as well
566 as in-frame deletions of *opgH* were constructed using the pTOX5 *cmR/msqR* allelic
567 exchange system[38]. Flanking regions were cloned into pTOX5 as described for
568 pCVD442. Conjugation was performed by mixing and pelleting equal parts of recipient
569 *V. cholerae* and donor MFD λ*pir*, and spotting onto LB + 1% glucose + 600μM DAP at
570 37°C for 5 hrs. The first round of selection was performed on LB + chloramphenicol (5 μg
571 μg ml^{-1}) + streptomycin + 1% glucose at 30°C. Chloramphenicol resistant colonies were

572 picked into a 96well plate containing 200μL LB + 1% glucose and incubated at 37°C
573 without agitation for 3 hrs, then counter selected on LB + 1% rhamnose at 30°C.
574 Mutations were verified by PCR.
575
576 Ectopic chromosomal expression from IPTG-inducible P_{tac} was achieved through use of
577 suicide vector pTD101, a pJL1[67] derivative carrying the P_{tac} promoter, a multiple cloning
578 site, and *lacIq* and integrates into the native *V. cholerae lacZ* (*vc2338*) locus. Single
579 genes of interest were amplified from N16961 genomic DNA, introducing a strong
580 consensus RBS (AGGAGA). Genes downstream of *mltG* (*vc2016, vc2015, vc2014*) were
581 amplified together maintaining their native organization, including 30bp upstream of
582 *vc2016* to retain the native RBS. Selection for double crossover events was performed
583 as described for pCVD442. Due to hypersensitivity of the Δ7 LTG strain to β-lactams,
584 ampicillin was reduced to 25 μg ml^{-1} for the first selection. Due to the osmosensitivity of
585 the Δ7 LTG strain, pTD101 in this strain (and control strains) was maintained as an ampR
586 single crossover without counterselection.
587
588 Suicide vector pAM299[68] was used to place *rlpA* under P_{ara} control at its native locus for
589 RlpA depletion experiments. pAM299 was introduced via conjugation and selection for
590 single crossover events on LB + kanamycin (50 μg ml^{-1}) + streptomycin. IPTG-inducible
591 overexpression of *rlpA-mCherry* fusions for localization studies and *sacB* for levan toxicity
592 assays was achieved using pHL100[68] or its conjugatable derivative pHL100mob. The
593 *sacB* gene was amplified from pCVD442.
594

595 ***Gene insertion/disruption assay for gene essentiality***

596 The suicide vector pAM224 was used to disrupt genes through single crossover
597 integration events. 300bp internal regions in the first third of each respective *orf* (towards
598 the 5' end) were cloned into pAM224 using methods described above. Quantitative
599 conjugation was performed by washing, mixing, and pelleting 500 µL of recipient *V.*
600 *cholerae* and donor MFD λ*pir*. Pellets were re-suspended in 50 µl of LB, spotted onto a
601 45 µm filter on LB + 600 µM DAP, and incubated at 37°C for 4 hrs. Cells were recovered
602 from the filters into 1 ml of LB by vigorous vortexing and 20 µl of the suspension was
603 reserved for 10-fold serial dilution and spotting onto LB + streptomycin (200 µg ml^{-1})
604 incubated at 30°C to calculate total CFU/ml for all viable *V. cholerae.* The remaining
605 suspension was pelleted and plated on LB + kanamycin (50 µg ml^{-1}) + streptomycin
606 incubated at 30°C. Viable CFU/ml were calculated, and kanamycin resistance was
607 verified by patching 50 colonies back onto LB + streptomycin +/- kanamycin (all kanR
608 colonies were patched if fewer than 50 colonies were recovered). Transformation
609 efficiency was calculated as a ratio of kanR CFU to all strepR CFU.

610

611 ***Western Blot Analysis***

612 Expression of translational mCherry fusions was induced in WT *V. cholerae* with 1 mM
613 IPTG in LB and grown to OD600 ~ 0.6. Cells were harvested by centrifugation (9500xg,
614 15 min) at room temperature and resuspended in 1% SDS + 10 mM dithiothreitol (DTT)
615 lysis buffer. Resuspended cells were incubated at 95°C for 3 min, then sonicated 4 x 5 s
616 at 20% amplitude. Standard western blots against mCherry were performed using
617 polyclonal mCherry antibody (Genetex #GTX59788) and detection by IRDye 800CW

618 secondary antibody (Li-cor #926-32211). After imaging for mCherry, the same blots were
619 then re-incubated with monoclonal RpoA antibody (BioLegend # 663104) detected by
620 IRDye 800CW secondary antibody on an Odyssey CLx imaging device (Li-cor).
621
622 ***Growth rate experiments***
623 Saturated overnight cultures used for growth curve experiments were washed once and
624 resuspended in final growth media, normalizing to OD_{600} 2.0. Normalized cell
625 suspensions were serially diluted into 200 µL growth media and incubated in a Bioscreen
626 growth plate reader (Growth Curves America) at 37°C with random shaking at maximum
627 amplitude, and OD_{600} recorded at 5-min intervals. Calculations of doublings per hour
628 (DPH) were performed in R as previously described[59]. Briefly, logarithmic regressions
629 were fitted to sections of growth curves with >5 consecutive values corresponding to
630 OD_{600} 0.03-0.1 (for 10^{-2} diluted inocula) or OD_{600} 0.01-0.1 (for $<10^{-3}$ diluted inocula).
631 Logarithmic regressions of ≥3 replicates with fit value $r^2 > 0.95$ were used to estimate
632 mean doublings per hour for each strain in each growth condition. Growth rates were not
633 calculated for samples that did not reach OD_{600} 0.1, either through absence of detectable
634 growth or lysis prior to reaching OD_{600} 0.1. Growth rates were also not calculated for
635 replicates that were subsequently determined to be suppressors or grew due to
636 irreproducible adaptation. Means within strains between dilution factors and between
637 strains within dilution factors were compared using a two-way Anova and Tukey HSD
638 post-hoc test.
639
640 ***Morphology analysis by microscopy***

641 Strains were grown as described in the figure legends and imaged without fixation on LB
642 0.8% agarose using a Leica DMi8 inverted microscope. Phase-contrast images were
643 analyzed using MicrobeJ. Default parameter settings were applied, and features (septa)
644 were defined as 25% constriction of cell width. Cell outlines were manually edited as
645 needed.
646
647 ***Sacculus composition analysis***
648 PG composition from insoluble sacculi samples were analyzed as described previously
649 with some modifications[69,70]. Briefly, cells were harvested and resuspended and in boiled
650 5% SDS for 1 h. Sacculi were repeatedly washed by ultracentrifugation (110,000 rpm,
651 10 min, 20ºC) with MilliQ water until SDS was totally removed. Samples were treated with
652 20 µg Proteinase K (1 h, 37 °C) for removal of Braun's lipoprotein, and finally treated with
653 muramidase (100 µg/mL) for 16 hours at 37 ºC. Muramidase digestion was stopped by
654 boiling and coagulated proteins were removed by centrifugation (14,000 rpm, 15 min).
655 For sample reduction, the pH of the supernatants was adjusted to pH 8.5-9.0 with sodium
656 borate buffer and sodium borohydride was added to a final concentration of 10 mg/mL.
657 After incubating for 30 min at room temperature, the samples pH was adjusted to pH 3.5
658 with orthophosphoric acid.
659
660 UPLC analyses of muropeptides were performed on a Waters UPLC system (Waters
661 Corporation, USA) equipped with an ACQUITY UPLC BEH C18 Column, 130Å, 1.7 µm,
662 2.1 mm X 150 mm (Waters, USA) and a dual wavelength absorbance detector. Elution of
663 muropeptides was detected at 204 nm. Muropeptides were separated at 45°C using a

664 linear gradient from buffer A (formic acid 0.1% in water) to buffer B (formic acid 0.1% in
665 acetonitrile) in an 18-minute run, with a 0.25 ml/min flow.
666
667 Relative total PG amount was calculated by comparison of the total intensities of the
668 chromatograms (total area) from three biological replicas normalized to the same OD600
669 and extracted with the same volumes. Muropeptide identity was confirmed by MS/MS
670 analysis, using a Xevo G2-XS QTof system (Waters Corporation, USA) (*see next section*
671 *for details*). Quantification of muropeptides was based on their relative abundances
672 (relative area of the corresponding peak) normalized to their molar ratio. Analyses were
673 performed in biological triplicates and means were compared with unpaired t-tests.
674
675 ***Soluble peptidoglycan analysis***
676 Sample preparation of soluble PG samples was performed as follows. Bacteria cultures
677 were harvested by centrifugation (4,000 rpm, 20 min, 4°C). Cell pellets were gently
678 resuspended and washed twice with ice-cold 0.9% NaCl solution. After pelleting the cells
679 again by centrifugation, they were resuspended in 1 ml water and boiled for 30 min.
680 Samples were centrifuged again to remove cell debris at 14,000 rpm for 15 min, and
681 soluble fractions were transferred to new tubes. Next, samples were filtered using 0.2 µm
682 pore size filters. Half of the sample was treated with muramidase (100 µg/mL) for 16 hours
683 at 37 ºC. Muramidase digestion was stopped by boiling and coagulated proteins were
684 removed by centrifugation (14,000 rpm, 15 min). Finally, sample pH was adjusted to pH
685 3.5 with orthophosphoric acid. When needed, samples were diluted or concentrated by
686 speed vacuum.

687

688 Soluble muropeptides were detected and characterized by MS/MS analysis, using a Xevo
689 G2-XS QTof system (Waters Corporation, USA) equipped with an ACQUITY UPLC BEH
690 C18 Column (130 Å, 1.7 µm, 2.1 mm x 150 mm (Waters, USA)). Muropeptides were
691 separated at 45 ºC using a linear gradient from buffer A (formic acid 0.1% in water) to
692 buffer B (formic acid 0.1% in acetonitrile) in an 18-min run, with a 0.25 ml/min flow. The
693 QTOF–MS instrument was operated in positive ionization mode. Detection of
694 muropeptides was performed by MS^E to allow for the acquisition of precursor and product
695 ion data simultaneously, using the following parameters: capillary voltage at 3.0 kV,
696 source temperature to 120 ºC, desolvation temperature to 350 ºC, sample cone voltage
697 to 40 V, cone gas flow 100 l/h, desolvation gas flow 500 l/h and collision energy (CE): low
698 CE: 6 eV and high CE ramp: 15-40 eV. Mass spectra were acquired at a speed of 0.25
699 s/scan. The scan was in a range of 100–2000 *m/z*. Data acquisition and processing was
700 performed using UNIFI software package (Waters Corp.).

701

702 An in-house compound library built in UNIFI was used for detection and identification of
703 muropeptides. Subsequent identification and confirmation of each muropeptide was
704 performed by comparison of the retention-times and mass spectrometric data to known
705 samples. Quantification was performed by integrating peak areas from extracted ion
706 chromatograms (EICs) of the corresponding *m/z* value of each muropeptide and
707 normalized to their molar ratio. Soluble muropeptide analyses were performed in
708 biological triplicates and means were compared with unpaired t-tests.

709

710 ***Antibiotic sensitivity***

711 For zone of inhibition assays, a lawn of saturated overnight culture was spread on an LB
712 plate and allowed to dry for 15 minutes. Filter disks (6 mm) were dropped with 5μL of
713 antibiotic solutions (Table S4) onto the lawns and incubated at 37°C for 24 hrs before
714 measurements. Means were compared with a one-way ANOVA and Tukey post-hoc test.

715

716 ***Fluorescent D-amino acid PG labeling***

717 Saturated overnight cultures were diluted 1:100 into LB with 100 μM BADA[49] at 37°C for
718 1.5 hrs before addition of antibiotic. Labeled samples were washed one time in LB before
719 imaging on LB 0.8% agarose pads using a Leica DMi8 inverted microscope set for 490
720 nm excitation.

721

722 Acknowledgements

723 We would like to acknowledge Dr. Stephen Zinder (Cornell University) for informative
724 comments based on his unique insight into bacterial physiology. We thank Dr. John
725 Helmann (Cornell University) and members of the Dörr lab for helpful comments on the
726 manuscript. Research on autolysins in the Dörr lab is funded by NIH R01 GM130971.
727 Research in the Cava lab is supported by MIMS, the Knut and Alice Wallenberg
728 Foundation (KAW), the Swedish Research Council and the Kempe Foundation. Research
729 in the VanNieuwenhze lab is supported by the NIH through R01 GM113172 and R35
730 GM136365.

731

732 References

1 Osawa, M. & Erickson, H. P. Turgor Pressure and Possible Constriction Mechanisms in Bacterial Division. *Frontiers in Microbiology* **9**, doi:10.3389/fmicb.2018.00111 (2018).
2 Cabeen, M. T. & Jacobs-Wagner, C. Bacterial cell shape. *Nature Reviews Microbiology* **3**, 601-610, doi:10.1038/nrmicro1205 (2005).
3 Egan, A. J. F., Errington, J. & Vollmer, W. Regulation of peptidoglycan synthesis and remodelling. *Nature Reviews Microbiology* **18**, 446-460, doi:10.1038/s41579-020-0366-3 (2020).
4 Zhao, H., Patel, V., Helmann, J. D. & Dörr, T. Don't let sleeping dogmas lie: new views of peptidoglycan synthesis and its regulation. *Mol Microbiol* **106**, 847-860, doi:10.1111/mmi.13853 (2017).
5 Sochacki, K. A., Shkel, I. A., Record, M. T. & Weisshaar, J. C. Protein diffusion in the periplasm of E. coli under osmotic stress. *Biophys J* **100**, 22-31, doi:10.1016/j.bpj.2010.11.044 (2011).
6 Cho, H. *et al.* Bacterial cell wall biogenesis is mediated by SEDS and PBP polymerase families functioning semi-autonomously. *Nat Microbiol* **1**, 16172, doi:10.1038/nmicrobiol.2016.172 (2016).
7 Leclercq, S. *et al.* Interplay between Penicillin-binding proteins and SEDS proteins promotes bacterial cell wall synthesis. *Scientific Reports* **7**, 43306, doi:10.1038/srep43306 (2017).
8 Taguchi, A. *et al.* FtsW is a peptidoglycan polymerase that is functional only in complex with its cognate penicillin-binding protein. *Nat Microbiol* **4**, 587-594, doi:10.1038/s41564-018-0345-x (2019).
9 Nambu, T., Minamino, T., Macnab, R. M. & Kutsukake, K. Peptidoglycan-Hydrolyzing Activity of the FlgJ Protein, Essential for Flagellar Rod Formation inSalmonella typhimurium. *Journal of Bacteriology* **181**, 1555-1561, doi:doi:10.1128/JB.181.5.1555-1561.1999 (1999).
10 Santin, Y. G. & Cascales, E. Domestication of a housekeeping transglycosylase for assembly of a Type VI secretion system. *EMBO Rep* **18**, 138-149, doi:10.15252/embr.201643206 (2017).
11 Höltje, J. V. Growth of the stress-bearing and shape-maintaining murein sacculus of Escherichia coli. *Microbiol Mol Biol Rev* **62**, 181-203, doi:10.1128/mmbr.62.1.181-203.1998 (1998).
12 Herlihey, F. A. & Clarke, A. J. in *Protein Reviews: Volume 17* (ed M. Zouhair Atassi) 41-56 (Springer Singapore, 2017).
13 Viollier, P. H. & Shapiro, L. A lytic transglycosylase homologue, PleA, is required for the assembly of pili and the flagellum at the Caulobacter crescentus cell pole. *Mol Microbiol* **49**, 331-345, doi:10.1046/j.1365-2958.2003.03576.x (2003).
14 Uehara, T. & Park, J. T. Growth of Escherichia coli: significance of peptidoglycan degradation during elongation and septation. *J Bacteriol* **190**, 3914-3922, doi:10.1128/jb.00207-08 (2008).
15 Nguyen, L. T., Gumbart, J. C., Beeby, M. & Jensen, G. J. Coarse-grained simulations of bacterial cell wall growth reveal that local coordination alone can be sufficient to maintain rod shape. *Proceedings of the National Academy of Sciences* **112**, E3689-E3698, doi:10.1073/pnas.1504281112 (2015).

16 Lee, T. K. & Huang, K. C. The role of hydrolases in bacterial cell-wall growth. *Current opinion in microbiology* **16**, 760-766, doi:10.1016/j.mib.2013.08.005 (2013).

17 Murphy, S. G. *et al.* Class A Penicillin-Binding Protein-Mediated Cell Wall Synthesis Promotes Structural Integrity during Peptidoglycan Endopeptidase Insufficiency in Vibrio cholerae. *mBio* **12**, doi:10.1128/mBio.03596-20 (2021).

18 Singh, S. K., SaiSree, L., Amrutha, R. N. & Reddy, M. Three redundant murein endopeptidases catalyse an essential cleavage step in peptidoglycan synthesis of Escherichia coli K12. *Mol Microbiol* **86**, 1036-1051, doi:10.1111/mmi.12058 (2012).

19 Byun, B. *et al.* Mechanism of the Escherichia coli MltE lytic transglycosylase, the cell-wall-penetrating enzyme for Type VI secretion system assembly. *Sci Rep* **8**, 4110, doi:10.1038/s41598-018-22527-y (2018).

20 Dik, D. A., Marous, D. R., Fisher, J. F. & Mobashery, S. Lytic transglycosylases: concinnity in concision of the bacterial cell wall. *Crit Rev Biochem Mol Biol* **52**, 503-542, doi:10.1080/10409238.2017.1337705 (2017).

21 Lee, M. *et al.* Exolytic and endolytic turnover of peptidoglycan by lytic transglycosylase Slt of Pseudomonas aeruginosa. *Proceedings of the National Academy of Sciences* **115**, 4393-4398, doi:10.1073/pnas.1801298115 (2018).

22 Vijayaraghavan, J. *et al.* Structural studies and molecular dynamics simulations suggest a processive mechanism of exolytic lytic transglycosylase from Campylobacter jejuni. *PLOS ONE* **13**, e0197136, doi:10.1371/journal.pone.0197136 (2018).

23 Höltje, J. V., Mirelman, D., Sharon, N. & Schwarz, U. Novel type of murein transglycosylase in Escherichia coli. *J Bacteriol* **124**, 1067-1076, doi:10.1128/jb.124.3.1067-1076.1975 (1975).

24 Williams, A. H. *et al.* A step-by-step in crystallo guide to bond cleavage and 1,6-anhydro-sugar product synthesis by a peptidoglycan-degrading lytic transglycosylase. *J Biol Chem* **293**, 6000-6010, doi:10.1074/jbc.RA117.001095 (2018).

25 Kraft, A. R., Templin, M. F. & Höltje, J. V. Membrane-bound lytic endotransglycosylase in Escherichia coli. *Journal of bacteriology* **180**, 3441-3447, doi:10.1128/JB.180.13.3441-3447.1998 (1998).

26 Bohrhunter, J. L., Rohs, P. D. A., Torres, G., Yunck, R. & Bernhardt, T. G. MltG activity antagonizes cell wall synthesis by both types of peptidoglycan polymerases in Escherichia coli. *Molecular Microbiology* **115**, 1170-1180, doi:https://doi.org/10.1111/mmi.14660 (2021).

27 Yunck, R., Cho, H. & Bernhardt, T. G. Identification of MltG as a potential terminase for peptidoglycan polymerization in bacteria. *Molecular Microbiology* **99**, 700-718, doi:10.1111/mmi.13258 (2016).

28 Sassine, J., Pazos, M., Breukink, E. & Vollmer, W. Lytic transglycosylase MltG cleaves in nascent peptidoglycan and produces short glycan strands. *The Cell Surface* **7**, 100053, doi:https://doi.org/10.1016/j.tcsw.2021.100053 (2021).

29 Tsui, H. C. *et al.* Suppression of a deletion mutation in the gene encoding essential PBP2b reveals a new lytic transglycosylase involved in peripheral peptidoglycan

824 synthesis in Streptococcus pneumoniae D39. *Mol Microbiol* **100**, 1039-1065,
825 doi:10.1111/mmi.13366 (2016).
826 30 Taguchi, A., Page, J. E., Tsui, H.-C. T., Winkler, M. E. & Walker, S. Biochemical
827 reconstitution defines new functions for membrane-bound glycosidases in
828 assembly of the bacterial cell wall. *Proceedings of the National Academy of*
829 *Sciences* **118**, e2103740118, doi:10.1073/pnas.2103740118 (2021).
830 31 Koraimann, G. Lytic transglycosylases in macromolecular transport systems of
831 Gram-negative bacteria. *Cell Mol Life Sci* **60**, 2371-2388, doi:10.1007/s00018-
832 003-3056-1 (2003).
833 32 Jacobs, C., Huang, L. J., Bartowsky, E., Normark, S. & Park, J. T. Bacterial cell
834 wall recycling provides cytosolic muropeptides as effectors for beta-lactamase
835 induction. *Embo j* **13**, 4684-4694 (1994).
836 33 Dik, D. A., Fisher, J. F. & Mobashery, S. Cell-Wall Recycling of the Gram-Negative
837 Bacteria and the Nexus to Antibiotic Resistance. *Chem Rev* **118**, 5952-5984,
838 doi:10.1021/acs.chemrev.8b00277 (2018).
839 34 Heidrich, C., Ursinus, A., Berger, J., Schwarz, H. & Holtje, J. V. Effects of multiple
840 deletions of murein hydrolases on viability, septum cleavage, and sensitivity to
841 large toxic molecules in Escherichia coli. *J Bacteriol* **184**, 6093-6099,
842 doi:10.1128/jb.184.22.6093-6099.2002 (2002).
843 35 Jorgenson, M. A., Chen, Y., Yahashiri, A., Popham, D. L. & Weiss, D. S. The
844 bacterial septal ring protein RlpA is a lytic transglycosylase that contributes to rod
845 shape and daughter cell separation in Pseudomonas aeruginosa. *Mol Microbiol*
846 **93**, 113-128, doi:10.1111/mmi.12643 (2014).
847 36 Weaver, A. I. *et al.* Lytic transglycosylases RlpA and MltC assist in Vibrio cholerae
848 daughter cell separation. *Molecular Microbiology* **112**, 1100-1115,
849 doi:10.1111/mmi.14349 (2019).
850 37 Priyadarshini, R., Popham, D. L. & Young, K. D. Daughter cell separation by
851 penicillin-binding proteins and peptidoglycan amidases in Escherichia coli. *Journal*
852 *of bacteriology* **188**, 5345-5355, doi:10.1128/JB.00476-06 (2006).
853 38 Lazarus, J. E. *et al.* A New Suite of Allelic-Exchange Vectors for the Scarless
854 Modification of Proteobacterial Genomes. *Appl Environ Microbiol* **85**,
855 doi:10.1128/aem.00990-19 (2019).
856 39 Deutscher, J. *et al.* The bacterial phosphoenolpyruvate:carbohydrate
857 phosphotransferase system: regulation by protein phosphorylation and
858 phosphorylation-dependent protein-protein interactions. *Microbiol Mol Biol Rev* **78**,
859 231-256, doi:10.1128/mmbr.00001-14 (2014).
860 40 Bontemps-Gallo, S., Bohin, J. & Lacroix, J. Osmoregulated Periplasmic Glucans.
861 *EcoSal Plus*, doi:doi:10.1128/ecosalplus.ESP-0001-2017 (2017).
862 41 Hill, N. S., Buske, P. J., Shi, Y. & Levin, P. A. A Moonlighting Enzyme Links
863 Escherichia coli Cell Size with Central Metabolism. *PLOS Genetics* **9**, e1003663,
864 doi:10.1371/journal.pgen.1003663 (2013).
865 42 Quintard, K. *et al.* Evaluation of the Role of the opgGH Operon in Yersinia
866 pseudotuberculosis and Its Deletion during the Emergence of Yersinia pestis.
867 *Infection and immunity* **83**, 3638-3647, doi:10.1128/IAI.00482-15 (2015).
868 43 Pereira, Y., Petit-Glatron, M.-F. & Chambert, R. yveB, encoding endolevanase
869 LevB, is part of the sacB–yveB–yveA levansucrase tricistronic operon in Bacillus

870 subtilis. *Microbiology* **147**, 3413-3419, doi:https://doi.org/10.1099/00221287-147-
871 12-3413 (2001).
872 44 Tanaka, T., Oi, S. & Yamamoto, T. The molecular structure of low and high
873 molecular weight levans synthesized by levansucrase. *J Biochem* **87**, 297-303,
874 doi:10.1093/oxfordjournals.jbchem.a132737 (1980).
875 45 Steinmetz, M., Le Coq, D., Djemia, H. B. & Gay, P. [Genetic analysis of sacB, the
876 structural gene of a secreted enzyme, levansucrase of Bacillus subtilis Marburg].
877 *Mol Gen Genet* **191**, 138-144, doi:10.1007/bf00330901 (1983).
878 46 Gay, P., Le Coq, D., Steinmetz, M., Ferrari, E. & Hoch, J. A. Cloning structural
879 gene sacB, which codes for exoenzyme levansucrase of Bacillus subtilis:
880 expression of the gene in Escherichia coli. *J Bacteriol* **153**, 1424-1431,
881 doi:10.1128/jb.153.3.1424-1431.1983 (1983).
882 47 Blomfield, I. C., Vaughn, V., Rest, R. F. & Eisenstein, B. I. Allelic exchange in
883 Escherichia coli using the Bacillus subtilis sacB gene and a temperature-sensitive
884 pSC101 replicon. *Molecular Microbiology* **5**, 1447-1457,
885 doi:https://doi.org/10.1111/j.1365-2958.1991.tb00791.x (1991).
886 48 Cho, H., Uehara, T. & Bernhardt, T. G. Beta-lactam antibiotics induce a lethal
887 malfunctioning of the bacterial cell wall synthesis machinery. *Cell* **159**, 1300-1311,
888 doi:10.1016/j.cell.2014.11.017 (2014).
889 49 Hsu, Y. P. *et al.* Full color palette of fluorescent d-amino acids for in situ labeling
890 of bacterial cell walls. *Chem Sci* **8**, 6313-6321, doi:10.1039/c7sc01800b (2017).
891 50 Kuru, E. *et al.* In Situ probing of newly synthesized peptidoglycan in live bacteria
892 with fluorescent D-amino acids. *Angew Chem Int Ed Engl* **51**, 12519-12523,
893 doi:10.1002/anie.201206749 (2012).
894 51 Dörr, T., Davis, B. M. & Waldor, M. K. Endopeptidase-mediated beta lactam
895 tolerance. *PLoS Pathog* **11**, e1004850, doi:10.1371/journal.ppat.1004850 (2015).
896 52 Weaver, A. I. *et al.* Genetic Determinants of Penicillin Tolerance in Vibrio cholerae.
897 *Antimicrob Agents Chemother* **62**, doi:10.1128/aac.01326-18 (2018).
898 53 Kuru, E. *et al.* Fluorescent D-amino-acids reveal bi-cellular cell wall modifications
899 important for Bdellovibrio bacteriovorus predation. *Nature Microbiology* **2**, 1648-
900 1657, doi:10.1038/s41564-017-0029-y (2017).
901 54 Hernández, S. B., Dörr, T., Waldor, M. K. & Cava, F. Modulation of Peptidoglycan
902 Synthesis by Recycled Cell Wall Tetrapeptides. *Cell Reports* **31**, 107578,
903 doi:https://doi.org/10.1016/j.celrep.2020.107578 (2020).
904 55 Barreteau, H. *et al.* Cytoplasmic steps of peptidoglycan biosynthesis. *FEMS*
905 *Microbiology Reviews* **32**, 168-207, doi:10.1111/j.1574-6976.2008.00104.x
906 (2008).
907 56 Dorr, T., Cava, F., Lam, H., Davis, B. M. & Waldor, M. K. Substrate specificity of
908 an elongation-specific peptidoglycan endopeptidase and its implications for cell
909 wall architecture and growth of Vibrio cholerae. *Mol Microbiol* **89**, 949-962,
910 doi:10.1111/mmi.12323 (2013).
911 57 Chaput, C., Labigne, A. & Boneca, I. G. Characterization of Helicobacter pylori lytic
912 transglycosylases Slt and MltD. *J Bacteriol* **189**, 422-429, doi:10.1128/jb.01270-06
913 (2007).

58 Scheurwater, E. M. & Clarke, A. J. The C-terminal Domain of Escherichia coli YfhD Functions as a Lytic Transglycosylase*. *Journal of Biological Chemistry* **283**, 8363-8373, doi:https://doi.org/10.1074/jbc.M710135200 (2008).

59 Mueller, E. A., Egan, A. J. F., Breukink, E., Vollmer, W. & Levin, P. A. Plasticity of Escherichia coli cell wall metabolism promotes fitness and antibiotic resistance across environmental conditions. *eLife* **8**, e40754, doi:10.7554/eLife.40754 (2019).

60 Yakhnina, A. A. & Bernhardt, T. G. The Tol-Pal system is required for peptidoglycan-cleaving enzymes to complete bacterial cell division. *Proceedings of the National Academy of Sciences* **117**, 6777-6783, doi:10.1073/pnas.1919267117 (2020).

61 Suzuki, M., Hara, H. & Matsumoto, K. Envelope disorder of Escherichia coli cells lacking phosphatidylglycerol. *J Bacteriol* **184**, 5418-5425, doi:10.1128/jb.184.19.5418-5425.2002 (2002).

62 Voedts, H. *et al.* Role of endopeptidases in peptidoglycan synthesis mediated by alternative cross-linking enzymes in Escherichia coli. *bioRxiv*, 2021.2002.2012.430937, doi:10.1101/2021.02.12.430937 (2021).

63 Heidelberg, J. F. *et al.* DNA sequence of both chromosomes of the cholera pathogen Vibrio cholerae. *Nature* **406**, 477-483, doi:10.1038/35020000 (2000).

64 Ferrières, L. *et al.* Silent mischief: bacteriophage Mu insertions contaminate products of Escherichia coli random mutagenesis performed using suicidal transposon delivery plasmids mobilized by broad-host-range RP4 conjugative machinery. *J Bacteriol* **192**, 6418-6427, doi:10.1128/jb.00621-10 (2010).

65 Gibson, D. G. *et al.* Enzymatic assembly of DNA molecules up to several hundred kilobases. *Nat Methods* **6**, 343-345, doi:10.1038/nmeth.1318 (2009).

66 Donnenberg, M. S. & Kaper, J. B. Construction of an eae deletion mutant of enteropathogenic Escherichia coli by using a positive-selection suicide vector. *Infection and immunity* **59**, 4310-4317, doi:10.1128/iai.59.12.4310-4317.1991 (1991).

67 Miyata, S. T., Unterweger, D., Rudko, S. P. & Pukatzki, S. Dual expression profile of type VI secretion system immunity genes protects pandemic Vibrio cholerae. *PLoS pathogens* **9**, e1003752-e1003752, doi:10.1371/journal.ppat.1003752 (2013).

68 Möll, A. *et al.* A D, D-carboxypeptidase is required for Vibrio cholerae halotolerance. *Environ Microbiol* **17**, 527-540, doi:10.1111/1462-2920.12779 (2015).

69 Alvarez, L., Hernandez, S. B., de Pedro, M. A. & Cava, F. in *Bacterial Cell Wall Homeostasis: Methods and Protocols* (ed Hee-Jeon Hong) 11-27 (Springer New York, 2016).

70 Desmarais, S. M., De Pedro, M. A., Cava, F. & Huang, K. C. Peptidoglycan at its peaks: how chromatographic analyses can reveal bacterial cell wall structure and assembly. *Mol Microbiol* **89**, 1-13, doi:10.1111/mmi.12266 (2013).

958 **Figures**

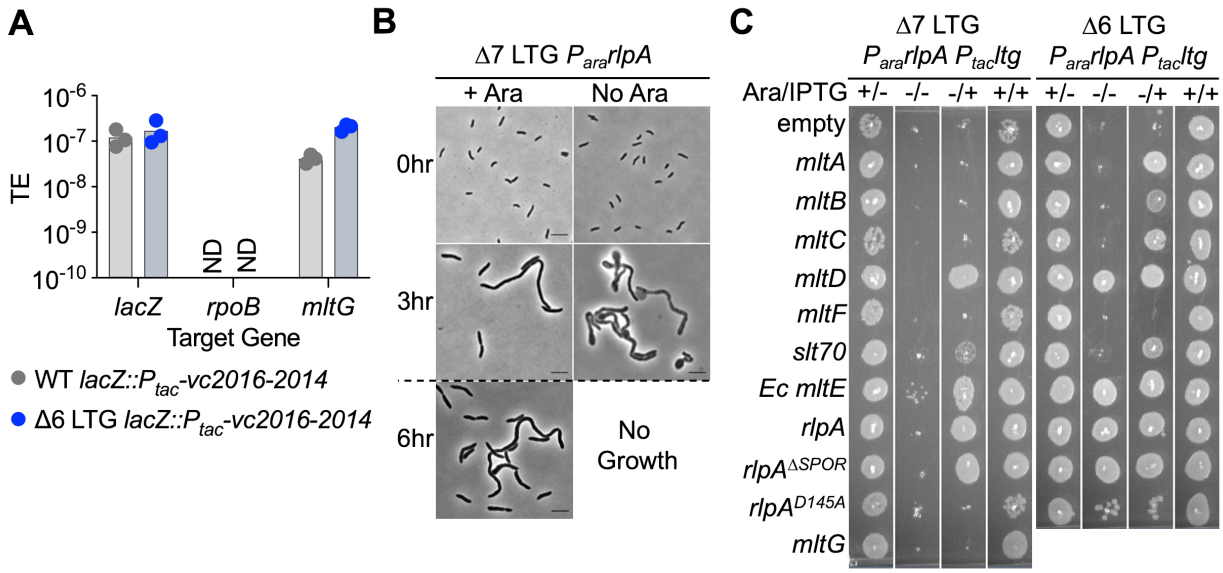

959

960 **Figure 1. A single LTG is necessary and sufficient for *V. cholerae* growth and**
961 **envelope homeostasis**
962 **(A)** *Trans* expression of DNA synthesis genes *vc2016-2014* permitted pAM299 disruption
963 of native *mltG* locus. *lacZ* and *rpoB* were targeted as positive and negative controls for
964 disruption, respectively. TE = Transformation Efficiency. ND = below limit of detection. 3
965 biological replicates are shown. **(B)** RlpA was depleted from the WT, Δ6, and Δ7 LTG
966 backgrounds by placing its native promoter under control of arabinose induction and
967 growing from a 10^{-3} overnight culture dilution into 5mL LB +/- 0.4% arabinose (ara) at 37
968 °C with shaking for 3 hrs, back-diluting 10^{-3} into fresh media, and incubating for another
969 3 hrs. Cells were imaged on LB agarose pads. Scale bars = 5μm. Dotted line indicates
970 10^{-3} back-dilution. **(C)** Arabinose-dependent RlpA depletion in Δ6 and Δ7 LTG
971 backgrounds was rescued with IPTG-inducible LTGs by growing cultures in LB +/- ara
972 (0.4%) and +/- IPTG (200μM) in 96 well plates at 37 °C without shaking for 3hrs, back-
973 diluting 10^{-3} into fresh media, incubating another 3 hrs, and spotting directly onto the same
974 media +kan50. Plates were incubated at 30 °C for 24hrs before imaging. Complete
975 plating efficiencies associated with panels (B) and (C) can be found in Figure 1 – Figure
976 Supplement 2 and Figure 1 – Figure Supplement 4, respectively. Images are
977 representative of 3 biological replicates.
978

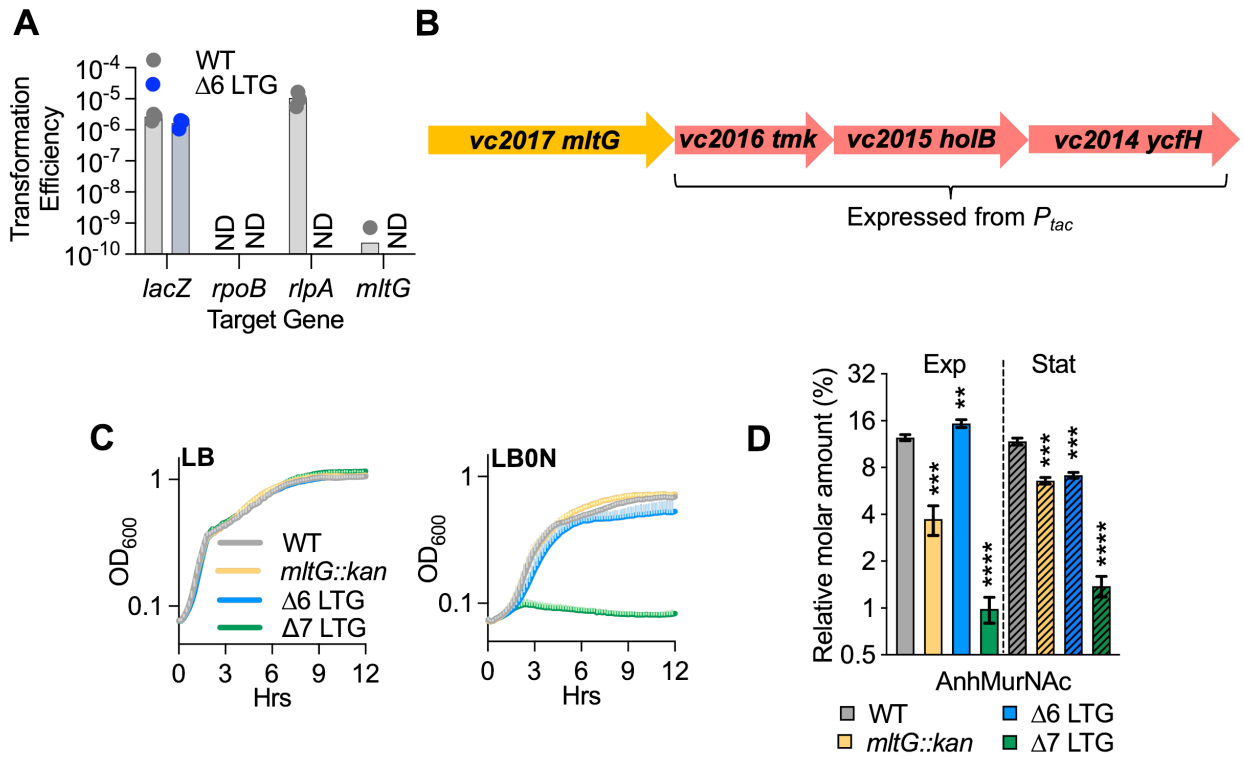

979
980 **Figure 1 – Figure Supplement 1. MltG is dispensable for growth of Δ6 LTG**
981 **(A)** Transformation efficiencies represent the strep^R and kan^R CFU divided by total viable
982 strep^R CFU recovered from a single mating. Streptomycin^R (Strep^R) *V. cholerae* WT and
983 Δ6 LTG strains were mated with a strep^S *E. coli* MFD donor strain carrying the pAM299
984 suicide vector carrying kanamycin resistance (Kan^R) and targeting positive control gene
985 *lacZ*, negative control gene *rpoB*, *rlpA*, or *mltG*. **(B)** The genetic region downstream of
986 *mltG* encodes essential DNA synthesis genes. **(C)** Mean growth curves for *mltG::kan*
987 strains in WT P_{tac}*vc2016-2014* and Δ6 LTG P_{tac}*vc2016-2014* backgrounds diluted 1:100
988 from overnight cultures into LB or LB0N and grown at 37°C. **(D)** Relative molar abundance
989 of all AnhMurNAc-containing muropeptide species in sacculus. Overnight cultures of WT,
990 *mltG::kan,* Δ6 LTG and Δ6 LTG *mltG::kan* (Δ7 LTG) in *lacZ::*P_{tac}*vc2016-2014*
991 backgrounds were diluted 1:100 into LB+200μM IPTG and samples collected for HPLC
992 analysis at OD_{600} 0.3 (Exp, solid bars) and OD_{600} 1.2 (Stat, striped bars). Complete
993 muropeptide profiles can be found in Supplemental File 1. Error bars represent standard
994 deviation from three biological replicates. Mutants were compared to the WT within each
995 growth phase with an unpaired t-test. ** = p<0.01, *** = p<0.001, **** = p<0.0001.
996

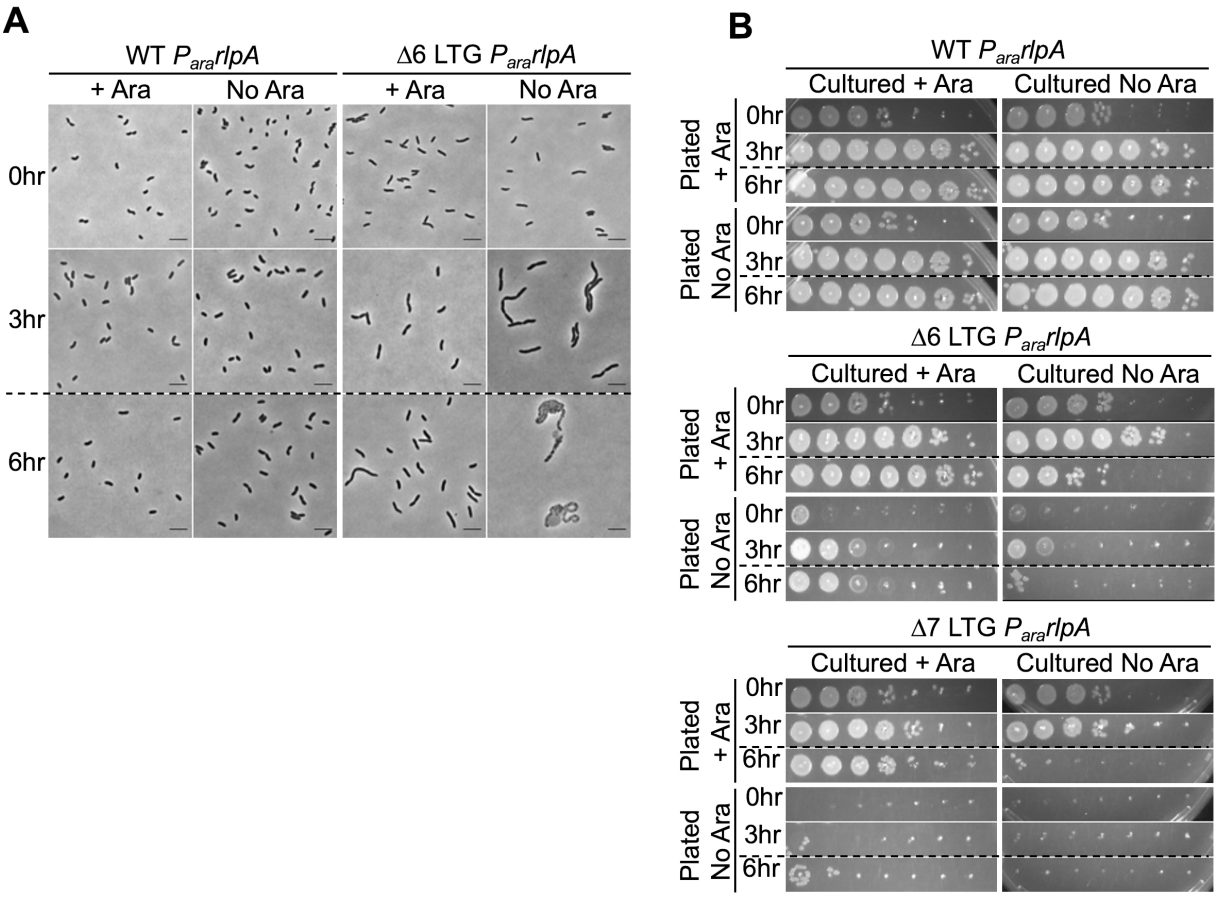

Figure 1 – Figure Supplement 2. RlpA depletion in the Δ6 and Δ7 LTG backgrounds. Native RlpA was depleted from the WT, Δ6, and Δ7 LTG backgrounds as described in Figure 1B, **(A)** imaged on LB agarose pads and **(B)** spot plated in 10-fold serial dilutions (10^0-10^{-6}) onto LB + kan50 +/- 0.4% arabinose and incubated at 30 °C for 24 hrs before imaging.

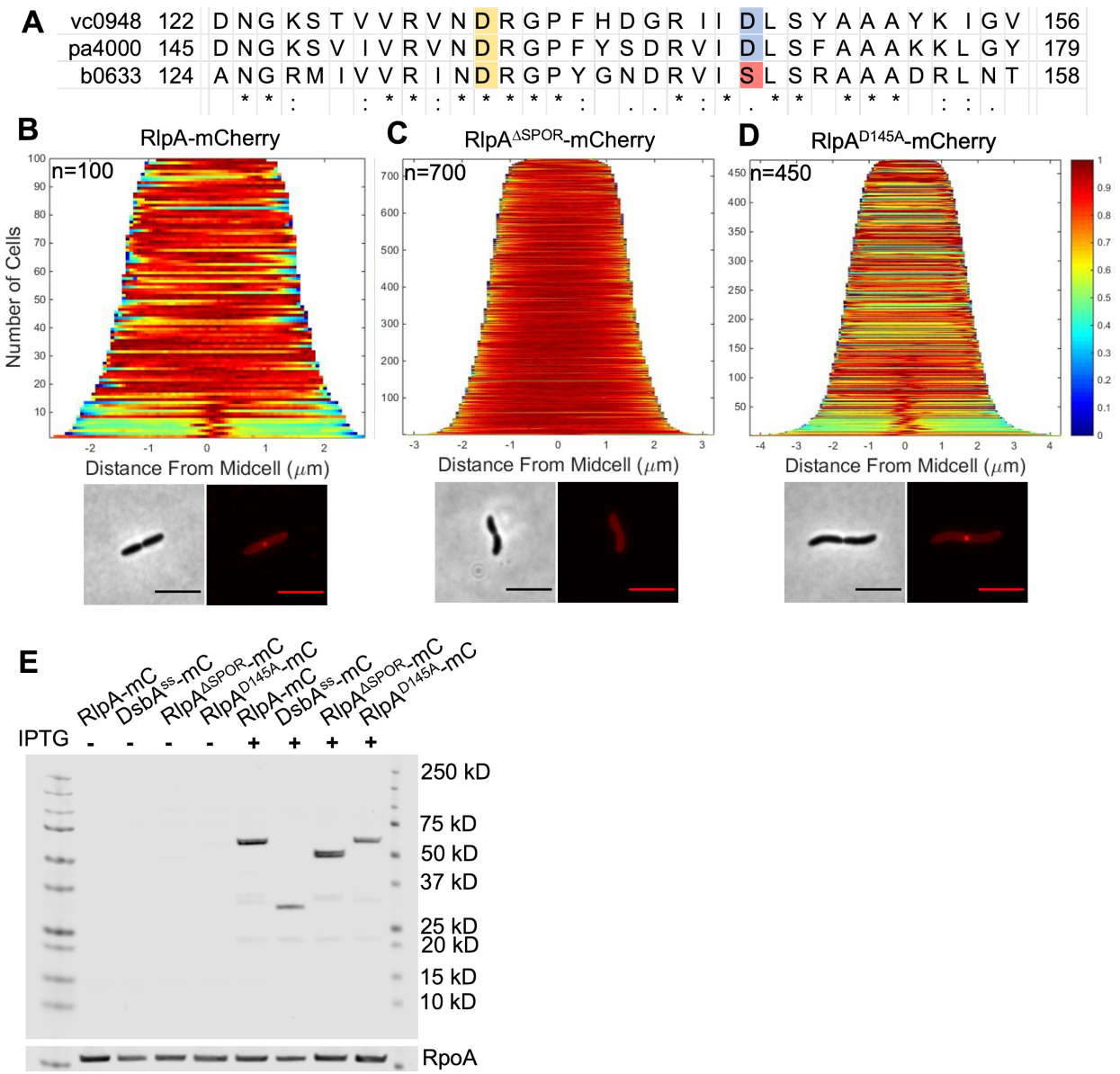

Figure 1 – Figure Supplement 3. RlpA active site architecture and localization

(A) Clustal Omega alignment of a relevant portion of lyase domain from *V. cholerae* RlpA (*vc0948*), *P. aeruginosa* RlpA (*pa4000*), and *E. coli* RlpA (*b0633*). Two Asp residues are implicated in PaRlpA activity: PaRlpA D156 aligns with VcRlpA D133 and EcRlpA D135, and PaRlpA D168 aligns with VcRlpA D145 and EcRlpA S147. WT *V. cholerae* carrying **(B)** pHL100 *rlpA-mCherry* **(C)** *rlpA$^{\Delta SPOR}$-mCherry* or **(D)** *rlpA^{D145A}-mCherry* was grown in M9 + 0.2% glucose at 30 °C for 2 hrs, induced with 1mM IPTG, and imaged on M9 + 0.2% glucose agarose pads at OD_{600} ~0.2. Demographs were generated using Oufti. Panels B-D are representative of 2 biological replicates. Scale bars = 5μm. **(E)** mCherry (mC) fusion proteins were detected with mCherry antibody, with mCherry fused to a DsbA signal sequence serving as a soluble mCherry size standard. RpoA loading control

1015 detected with RpoA antibody. Raw and unedited blots can be found in Figure 1 – Source
1016 Data 1.

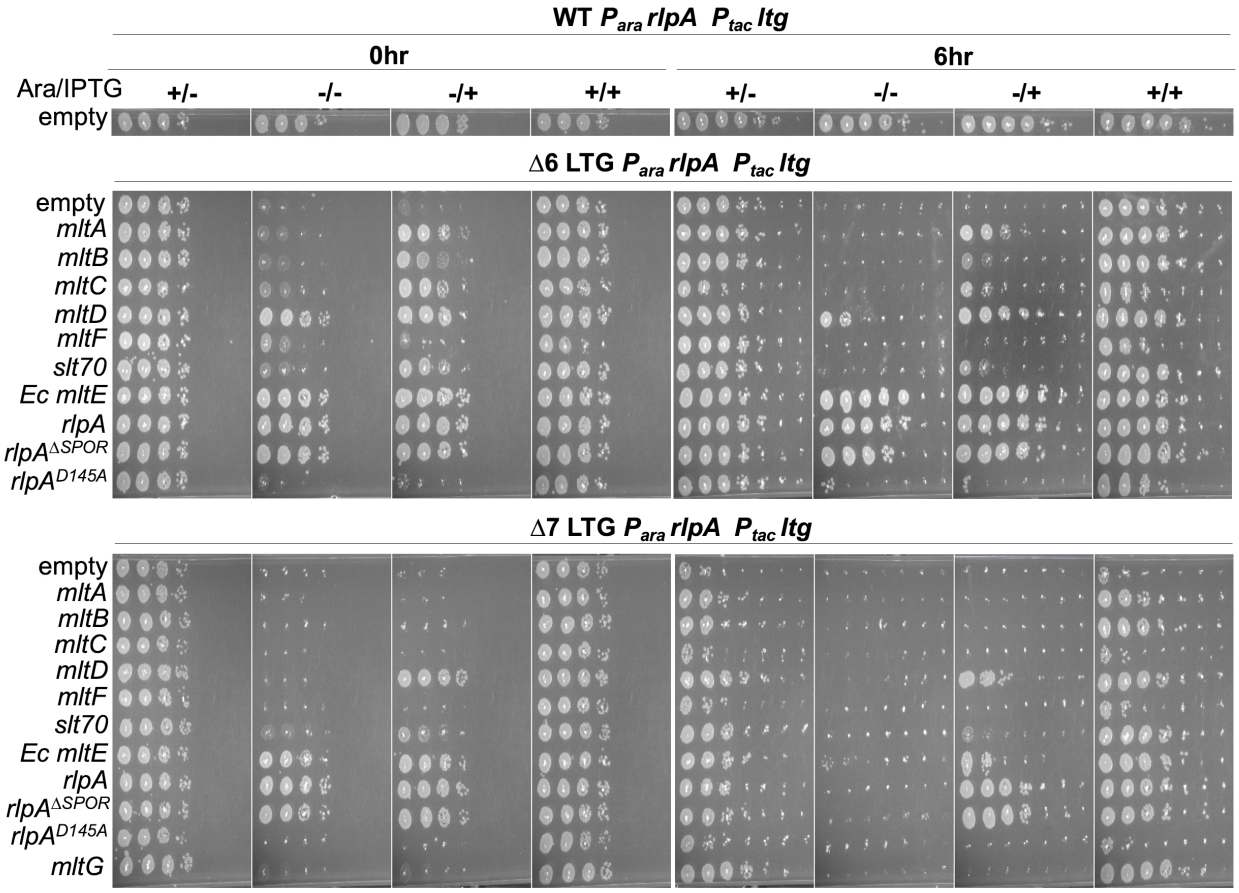

1017
1018 **Figure 1 – Figure Supplement 4. LTGs have variable ability to sustain growth**
1019 Native RlpA depletion in Δ6 and Δ7 LTG backgrounds was rescued by single LTGs as
1020 described in Figure 1B, spot plated in 10-fold serial dilutions (from 10^0-10^{-6}) at 0 hrs and
1021 6 hrs, then incubated at 30 °C for 24hrs before imaging. Images are representative of 3
1022 biological replicates.
1023
1024 **Figure 1 – Source Data 1. Raw and uncropped mCherry Western blots**
1025

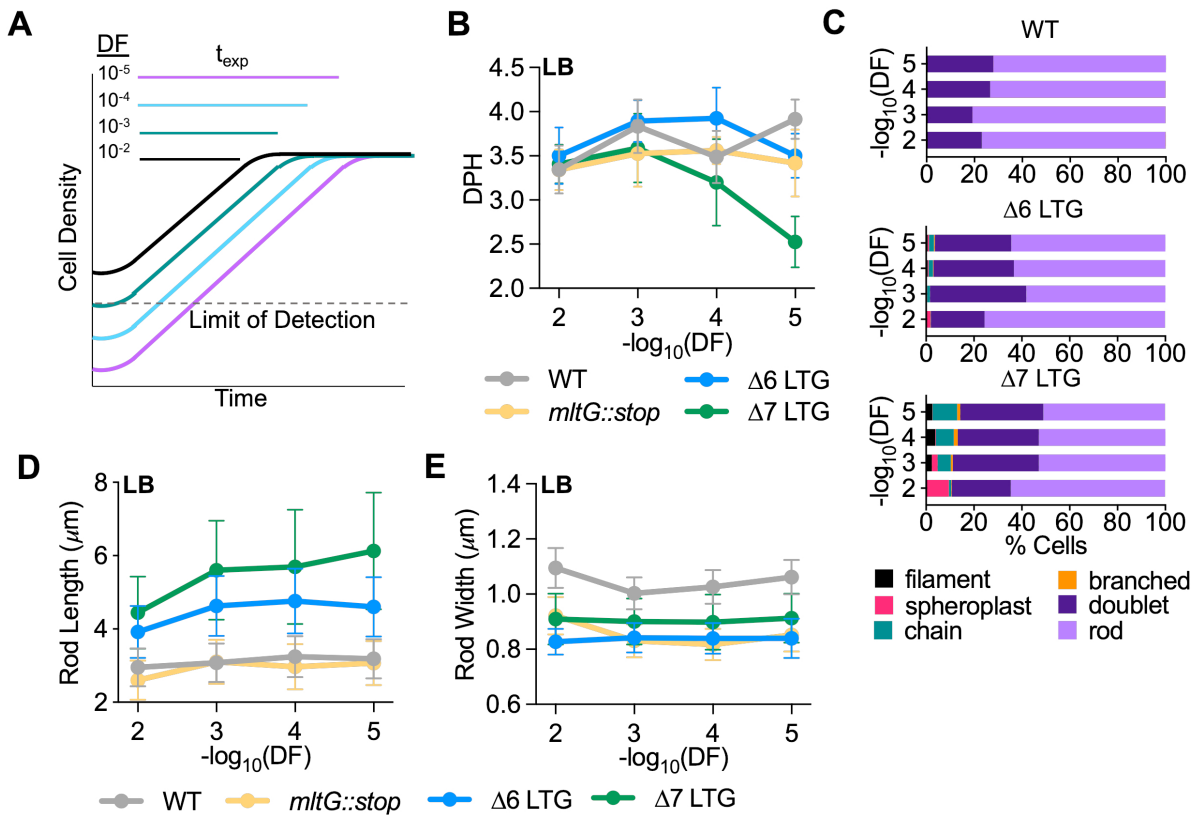

Figure 2. LTG insufficiency causes cumulative growth and morphology defects
(A) Schema describing relationship between dilution factor (DF) of saturated cultures into fresh media and time spent in exponential growth (t_{exp}). **(B)** Mass doubling times (doublings per hour, DPH) from growth curves performed in LB inoculated with 10-fold serial dilutions of saturated overnight cultures. Values were calculated from growth curves shown in Figure 2 – Figure Supplement 2. Error bars represent standard deviation of the mean, n≥3. **(C)** Relative abundance of cell morphologies from cultures at OD_{600} 0.3 from panel C. n>500 cells. Definition criteria and images are shown in Figure 2 – Figure Supplement 1. Mean length **(D)** and width **(E)** as a function of dilution factor (DF) of rod cells from panel (C). n>500 rods.

A

Morphology	Features	Poles	Septa	Length
Spheroplast	Round	N/A	N/A	N/A
Branched	N/A	3+	0+	N/A
Rod	N/A	2	0	less than 2x the median length of cells with 0 septa
Filament	N/A	2	0	greater than 2x the median length of cells with 0 septa
Doublet	N/A	2	1	N/A
Chain	N/A	2	2+	N/A

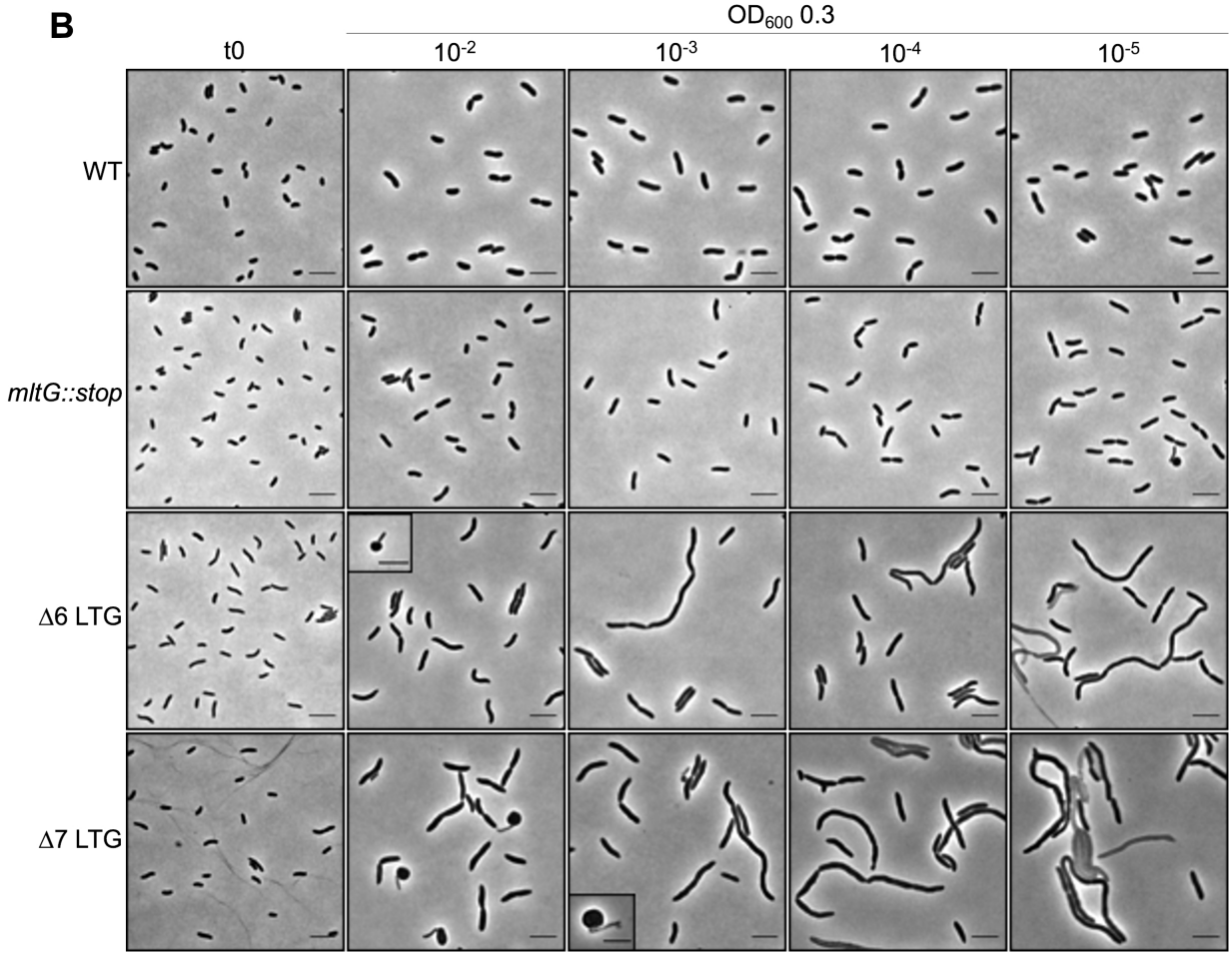

Figure 2 – Figure Supplement 1. Definitions of morphology defect categories
(A) Cell morphology classification criteria. **(B)** Representative micrographs of cell morphologies where each cell type depicted accounts for >1% of population as sampled from cultures grown in LB to OD_{600} 0.3 from 10-fold serial dilutions of overnight cultures. Scale bars = 5 μm.

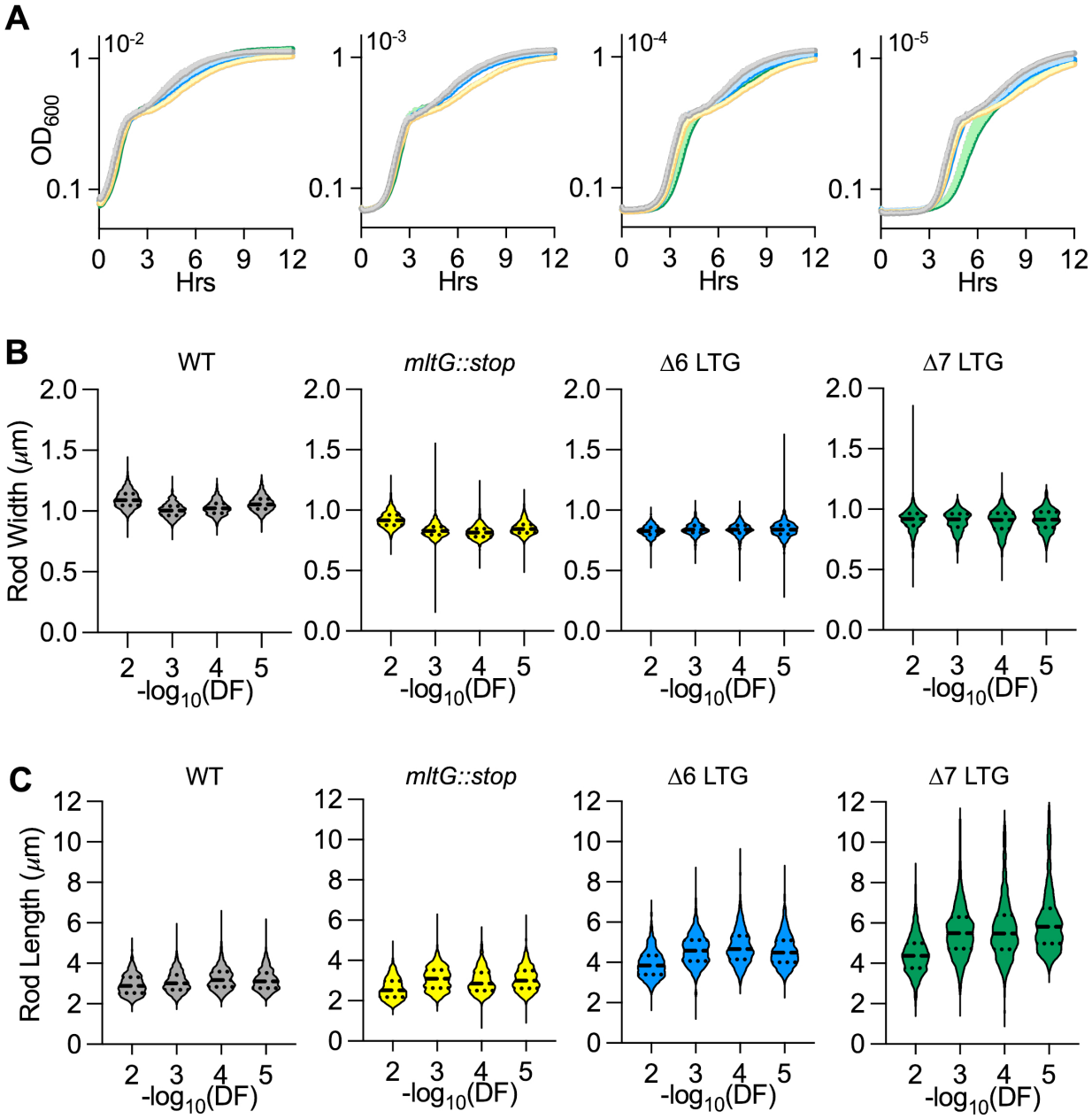

Figure 2 – Figure Supplement 2. Quantitative growth and morphology of LTG-deficient mutants in LB during extended exponential phase

(A) Growth curves were performed in LB at 37°C inoculated with 10-fold serial dilutions of saturated overnight cultures. Violin plots of raw **(B)** mean width or **(C)** length of single rods. n > 500 single rods. Error bars represent standard deviation of the mean, n≥3. DF = Dilution Factor

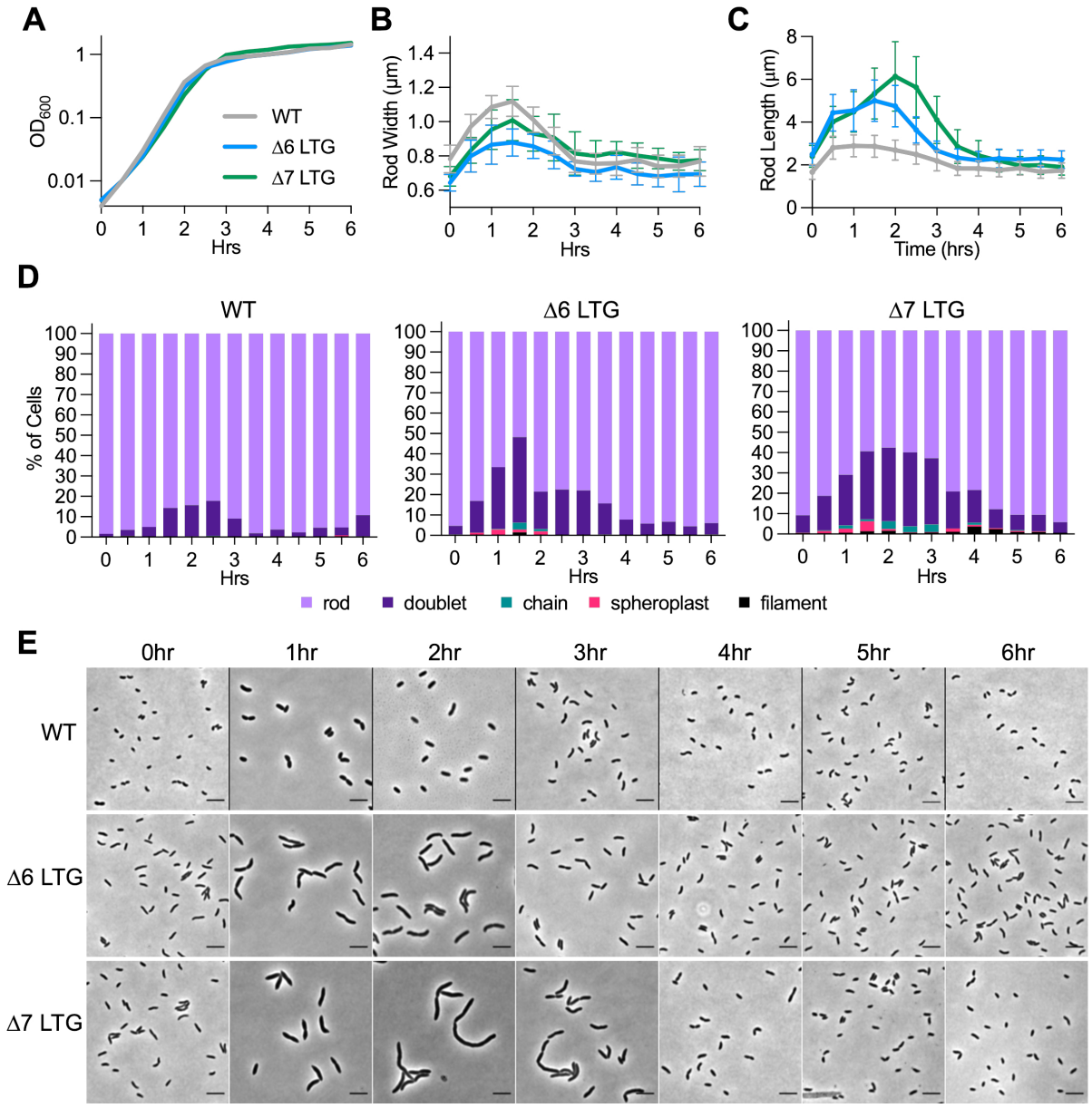

Figure 2 – Figure Supplement 3. Morphology of LTG-deficient mutants in LB is growth-phase dependent.

Saturated overnight cultures were diluted 1/1000 into LB at 37 °C and periodically sampled for **(A)** OD_{600} and imaged on LB agarose pads for **(B)** mean width, **(C)** length, and **(D)** cell morphology as exhibited in **(E)** representative micrographs. Error bars in (B) and (C) represent standard deviation of the mean, n >1 00 single rods. n > 200 cells for (D). Scale bars = 5µm.

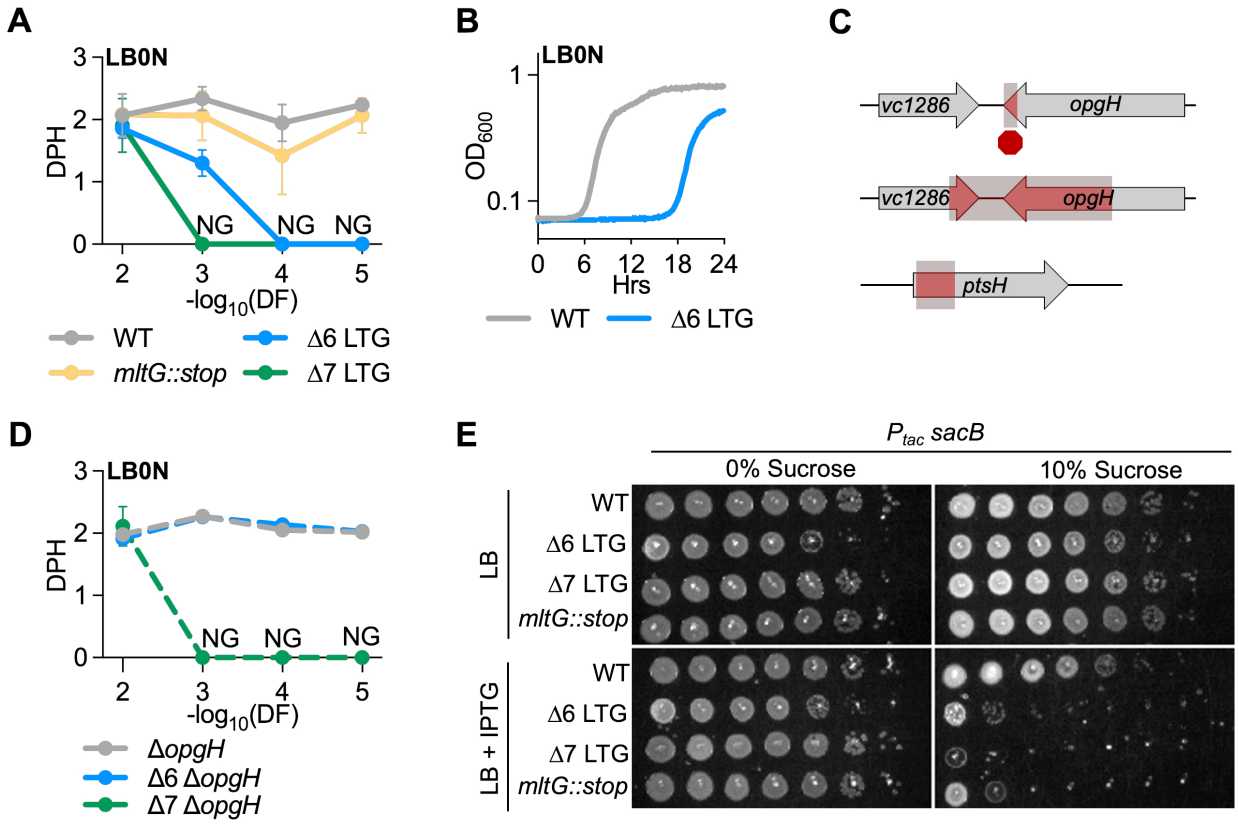

Figure 3. LTG mutants are hypersensitive to low osmolarity and accumulation of periplasmic polymers

(A) Mass doublings (doublings per hour, DPH) upon increasing dilutions (DF, dilution factor) during growth in LB0N. Values were calculated from growth curves in Figure 3 – Figure Supplement 1. Error bars represent standard deviation of the mean, n≥3. NG, no growth **(B)** Representative growth curve in low-salt LB (LB0N) showing late-growing spontaneous suppressor in Δ6 LTG **(C)** Whole genome sequencing of Δ6 LB0N suppressor mutations identify a premature stop resulting in a 6% 3' truncation of *opgH;* a deletion resulting in a 56% 3' truncation of *opgH* and 36% 3' truncation of *vc1286;* and a deletion of the 5' end of *ptsH*. **(D)** Validation of low osmolarity growth defect suppression by an *opgH* mutation. Shown are mass doublings (doublings per hour, DPH) upon increasing dilutions (DF, dilution factor) during growth in LB0N. Values were calculated from growth curves shown in Figure 3 – Figure Supplement 1 **(E)** Saturated overnight cultures harboring IPTG-inducible *sacB* were 10-fold serially diluted and plated on LB+kan50 +/- 200μM IPTG +/- 10% sucrose, incubated at 30 °C, and imaged 24 hrs before. Representative of 3 biological replicates. Empty vector and LB0N controls are shown in Figure 3 – Figure Supplement 4.

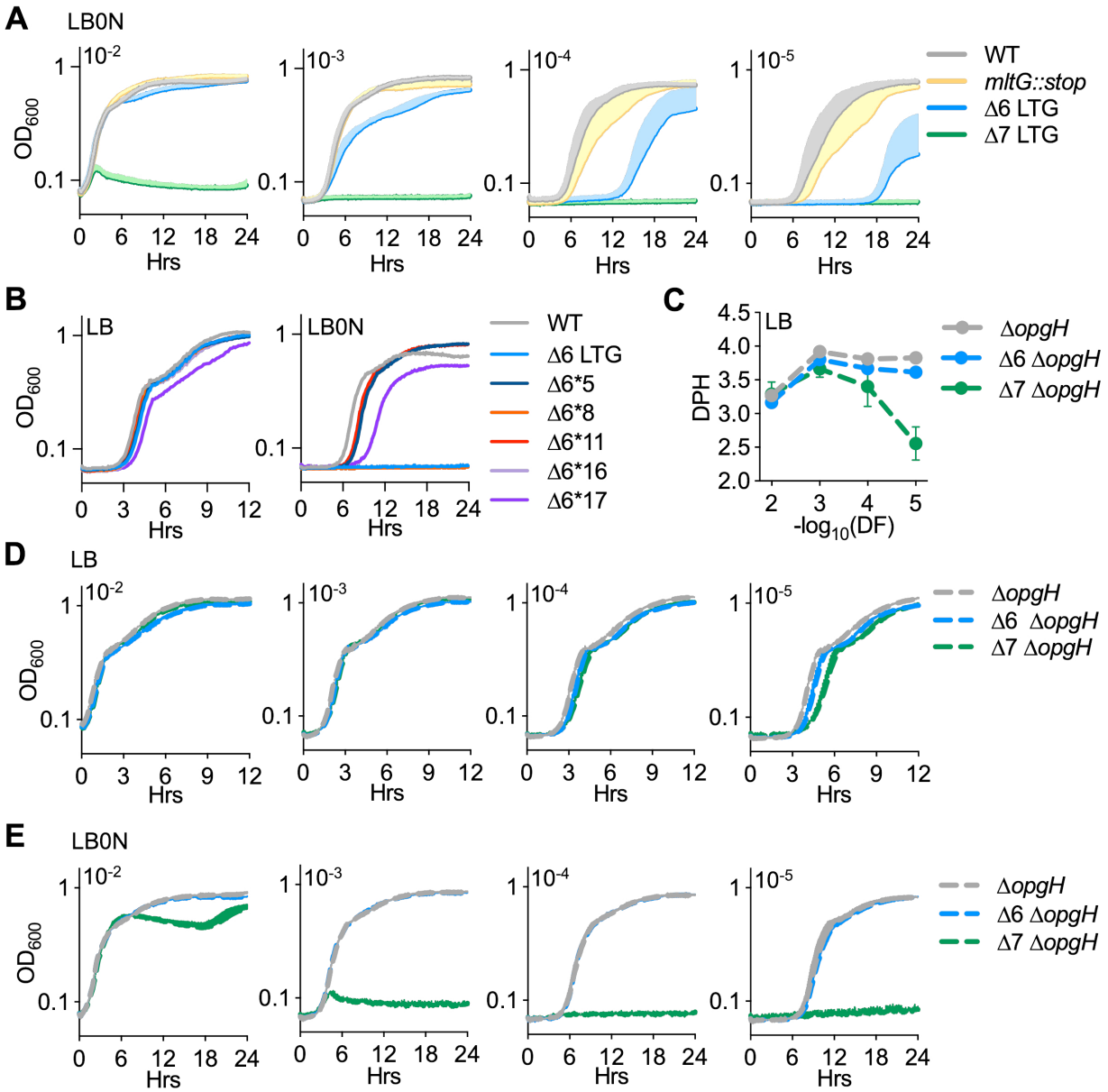

Figure 3 – Figure Supplement 1. Suppression of growth defects of ΔLTG mutants in low salt LB

(A) Mean growth curves in LB0N at 37°C started from 10-fold dilutions of saturated overnight cultures used to generate growth rates in Figure 3A. Error bars = positive standard deviation of the mean, n > 3. Growth plot on the right is reproduced from Figure 3 for comparison **(B)** Suppressors of the Δ6 LTG LB0N growth defect were isolated on LB and then tested for growth in LB and LB0N from a 10^{-5} inoculum of saturated overnight (LB) culture. **(C)** Mass doubling times of Δ*opgH* mutants calculated from **(D)** growth curves of Δ*opgH* mutants in LB at 37°C inoculated with 10-fold serial dilutions of saturated overnight cultures. **(E)** Mean growth curves in LB0N at 37°C started from 10-fold dilutions

of saturated overnight cultures used to generate growth rates in Figure 3D. error bars = standard deviation of the mean, n=3.

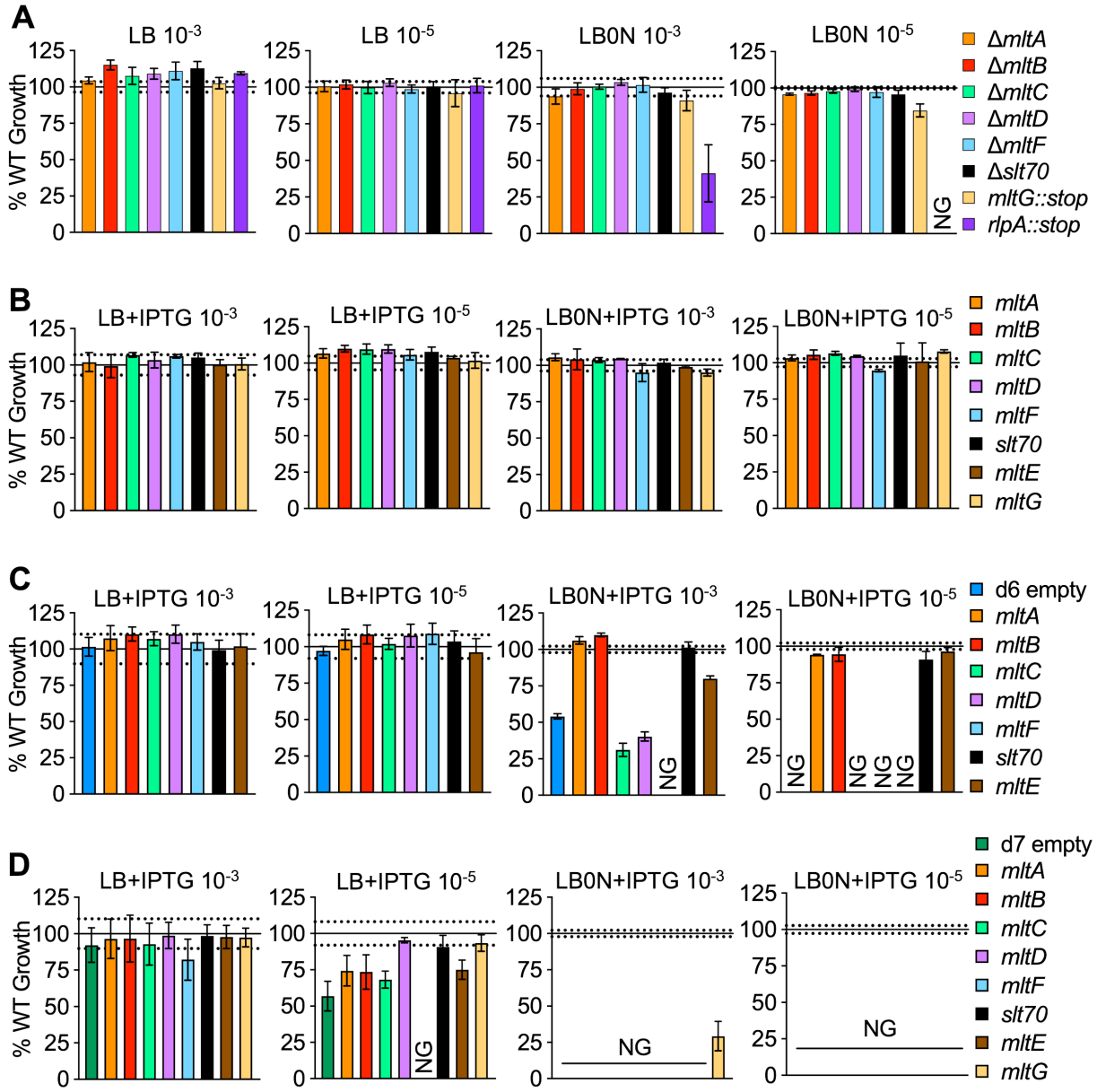

Figure 3 – Figure Supplement 2. Single LTG contributions to growth in LB and low salt LB.

Mass doubling times of strains diluted 10^{-3} or 10^{-5} into LB and LB0N (+ 200μM IPTG when induction was required) normalized to the appropriate WT controls under the same growth conditions. Solid line = WT mean, Dotted lines = +/- standard deviation of WT mean. **(A)** Single LTG mutant growth normalized to WT growth. **(B)** WT, **(C)** Δ6 LTG and **(D)** Δ7 LTG carrying chromosomal *lacZ::P*$_{tac}$ *ltg* normalized to WT *lacZ::P*$_{tac}$ empty. Experiments in panels (c) and (d) were carried out simultaneously and therefore share the same control

replicates. Error bars represent standard deviation of 3 biological replicates. NG = No Growth. Raw curves for (A-D) and uninduced data for (B-D) available in Figure 3 – Source Data 1.

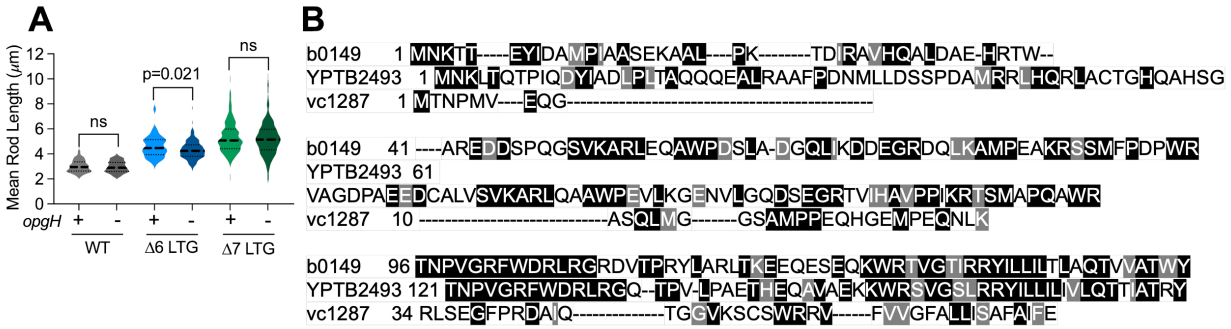

Figure 3 – Figure Supplement 3. Periplasmic glucans do not contribute to division defects in ΔLTG mutants

(a) Δ*opgH* mutants in WT, Δ6, and Δ7 backgrounds were grown in LB at 37 °C to OD_{600} 0.3 from 10^{-3} inoculum of saturated overnight culture, imaged on LB agarose pads, and single rod lengths analyzed in MicrobeJ. Dotted lines denote quartiles. Significance determined by unpaired Mann-Whitney tests, n>70 single rods. **(b)** T-Coffee alignment of predicted cytoplasmic N-terminal domains from *E. coli* OpgH (*b0149*), *Y. pseudotuberculosis* MdoH (*yptb2493*), and *V. cholerae* OpgH (*vc1287*).

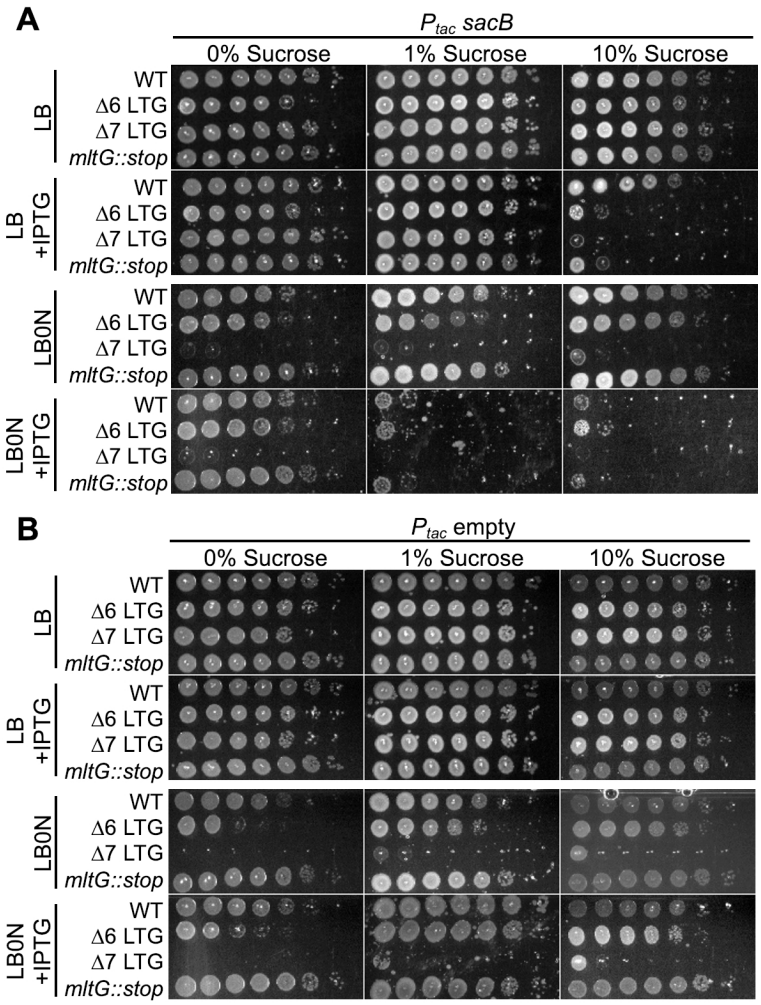

Figure 3 – Figure Supplement 4. SacB expression is toxic in ΔLTG mutants in a sucrose-dependent manner.

Saturated overnight cultures harboring **(a)** IPTG-inducible *sacB* or **(b)** empty vector were 10-fold serially diluted (10^0-10^{-6}) and plated on LB+kan50 and LB0N+kan50 +/- IPTG (200μM) + sucrose (0, 1,or 10% W/V) and incubated at 30 °C for 24 hrs before imaging. Representative of 3 biological replicates.

Figure 3 – Source Data 1. Raw growth curve data for single LTG mutants and LTG complementation in LTG-deficient mutants.

Presents raw OD_{600} measurements for growth curves performed in LB and low-salt LB (LB0N) with and without induction of *trans*-complementation by single LTGs in LTG-deficient mutant backgrounds, as well as growth curves in LB and LB0N of single LTG-deficient mutants. n≥3

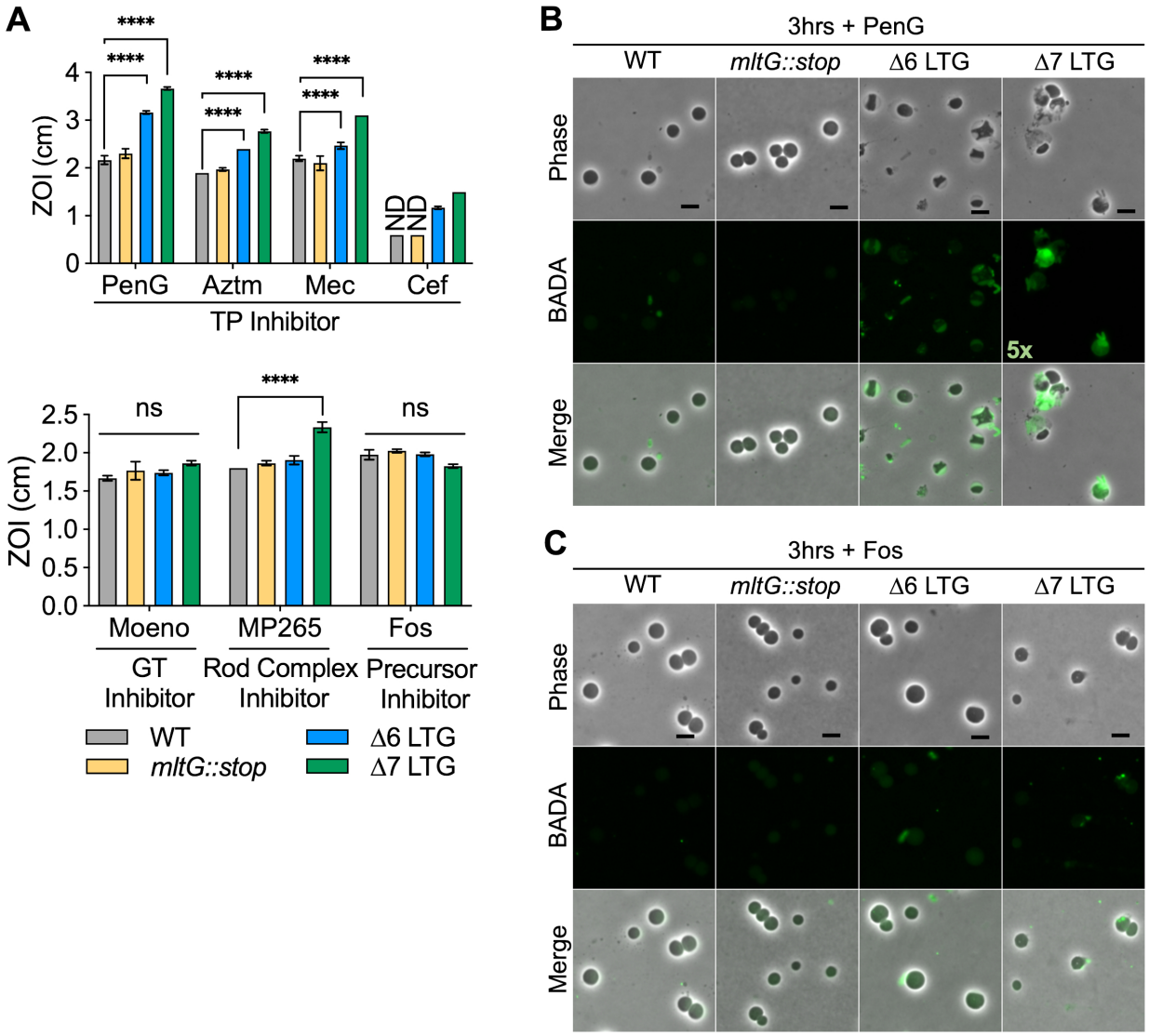

Figure 4. LTG mutants are hypersensitive to antibiotics promoting periplasmic PG accumulation

(A) Sensitivity to Penicillin G (PenG), aztreonam (AZTM), mecillinam (Mec), cefsulodin (Cef), moenomycin (Moeno), MP265, and Fosfomycin (Fos) measured as Zone of Inhibition (ZOI) in a disk diffusion assay. ND = No ZOI around disk. Error bars = standard deviation. Significance determined by one-way Anova. ns = $p>0.05$, * = $p< 0.05$, ** = $p<0.01$, *** = $p<0.001$, **** = $p<0.0001$. Overnight cultures were diluted 1:100 into LB+BADA (100μM) and grown at 37°C to OD_{600} 0.5 before addition of **(B)** PenG (100μg ml^{-1}) or **(C)** Fosfomycin (500μg ml^{-1}). Resulting spheroplasts were washed and imaged after 3hrs of antibiotic exposure. Fluorescence was normalized to the same intensity threshold for visual comparison except where indicated (Exceptionally bright samples were normalized to a higher intensity threshold denoted by the multiplier). Representative of 2 biological replicates. Scale bar = 5μm

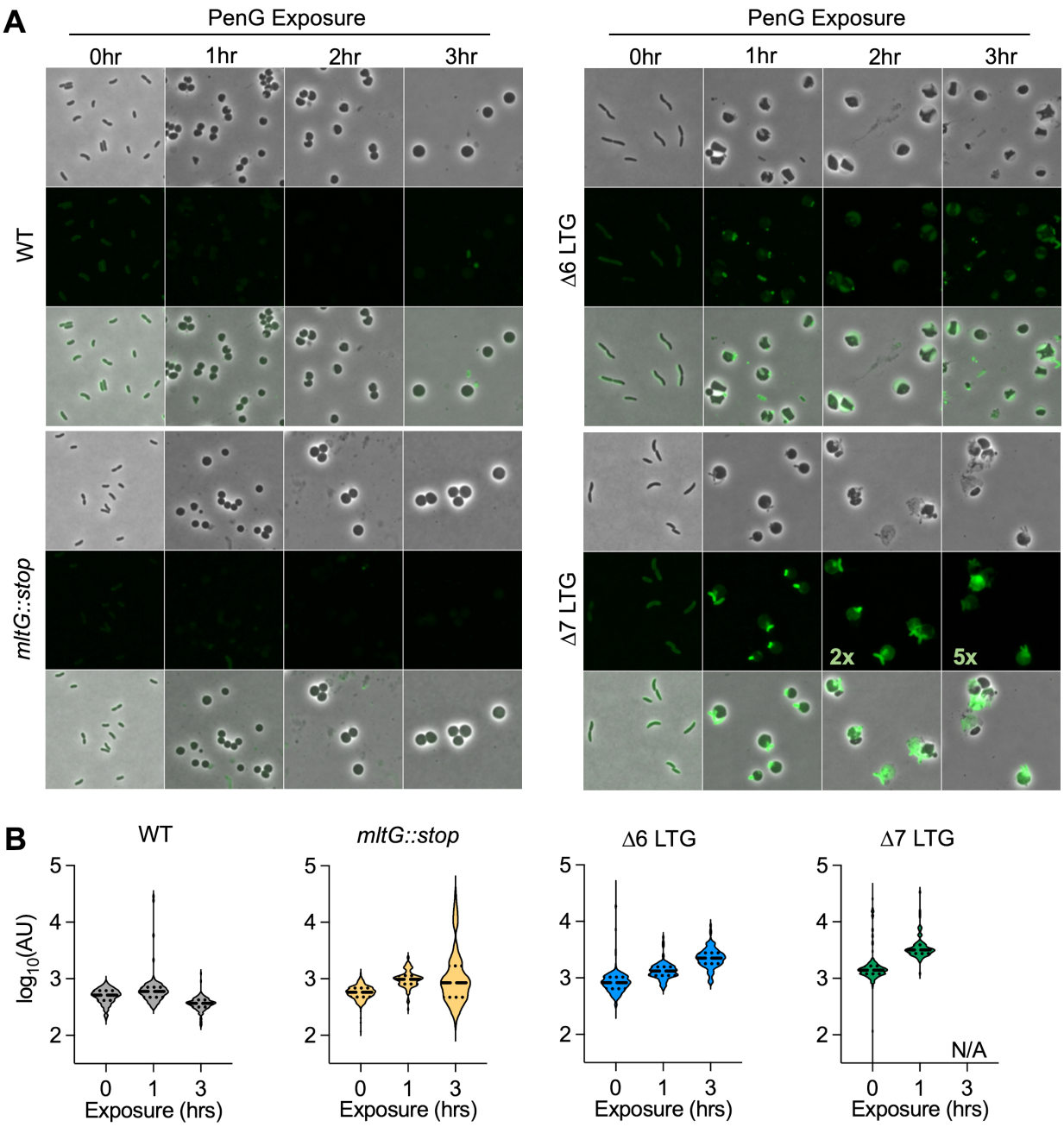

Figure 4 – Figure Supplement 1. Periplasmic cell wall accumulation in response to Penicillin G.

Overnight cultures were diluted 1:100 into LB+BADA (100μM) and grown at 37°C to OD_{600}0.5 before addition of PenG (100μg ml^{-1}). Resulting spheroplasts were removed periodically, washed, and imaged on LB agarose. **(A)** Fluorescence was normalized to the same intensity threshold in Figure 4 – Figure Supplement 1 and Figure 4 – Figure Supplement 2 for comparison except where indicated (Exceptionally bright samples were normalized to a higher intensity threshold denoted by the multiplier). Representative of 2 biological replicates. Scale bar = 5μm **(B)** Mean fluorescence intensity (AU) for >100 cells

1150 or spheroplasts were measured in ImageJ. N/A = not applicable due to insufficient intact
1151 spheroplasts for measurement.
1152

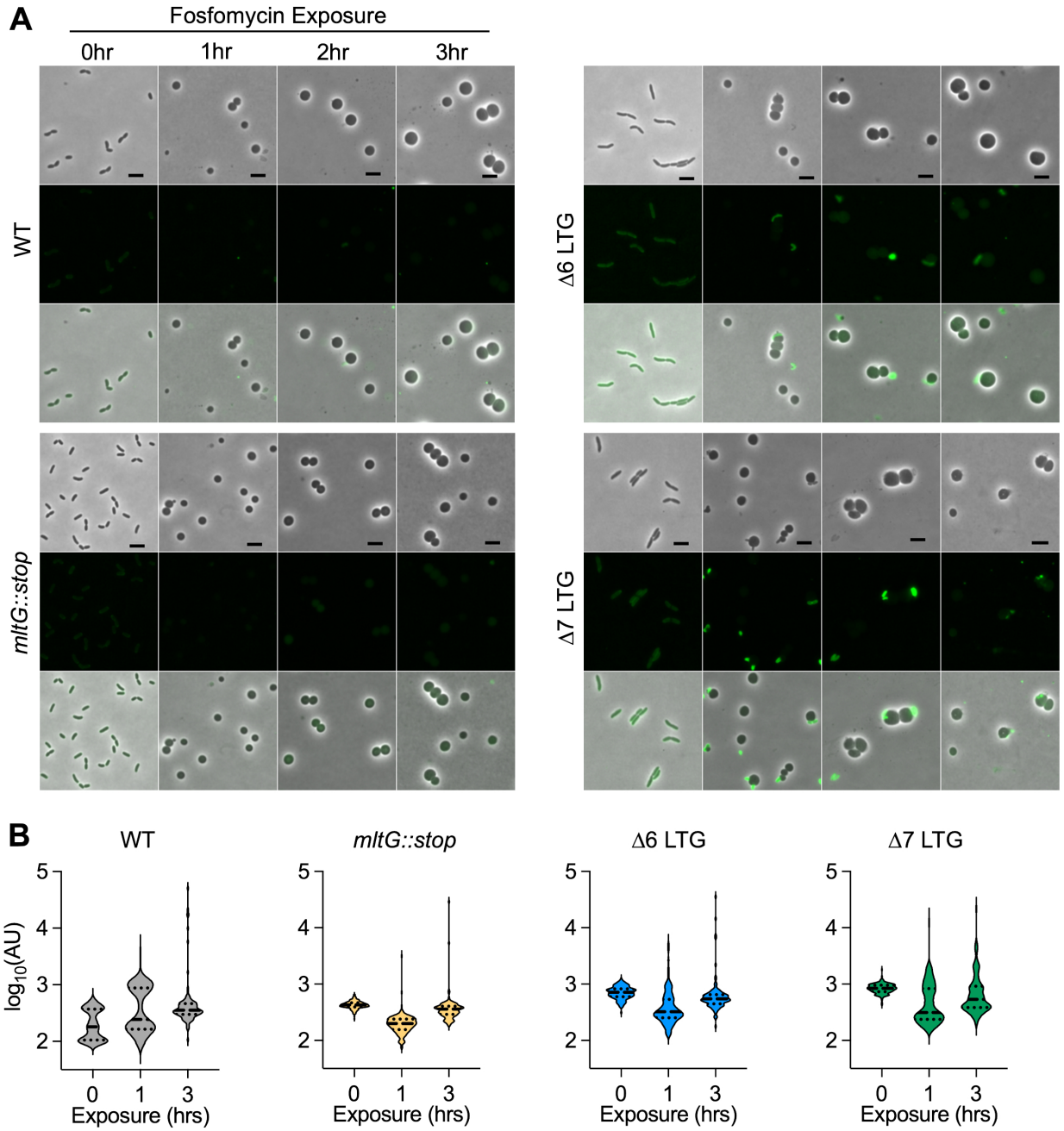

1153
1154 **Figure 4 – Figure Supplement 2. Lack of periplasmic cell wall accumulation in**
1155 **response to Fosfomycin.**
1156 Overnight cultures were diluted 1:100 into LB+BADA (100μM) and grown at 37°C to
1157 OD_{600}0.5 before addition of Fosfomycin (500μg ml^{-1}). Resulting spheroplasts were
1158 removed periodically, washed, and imaged on LB agarose. **(A)** Fluorescence was
1159 normalized to the same intensity threshold in Figure 4 – Figure Supplement 1 and Figure

4 – Figure Supplement 2 for comparison. Representative of 2 biological replicates. Scale bar = 5μm. **(B)** Mean fluorescence intensity (AU) for >100 cells or spheroplasts were measured in ImageJ.

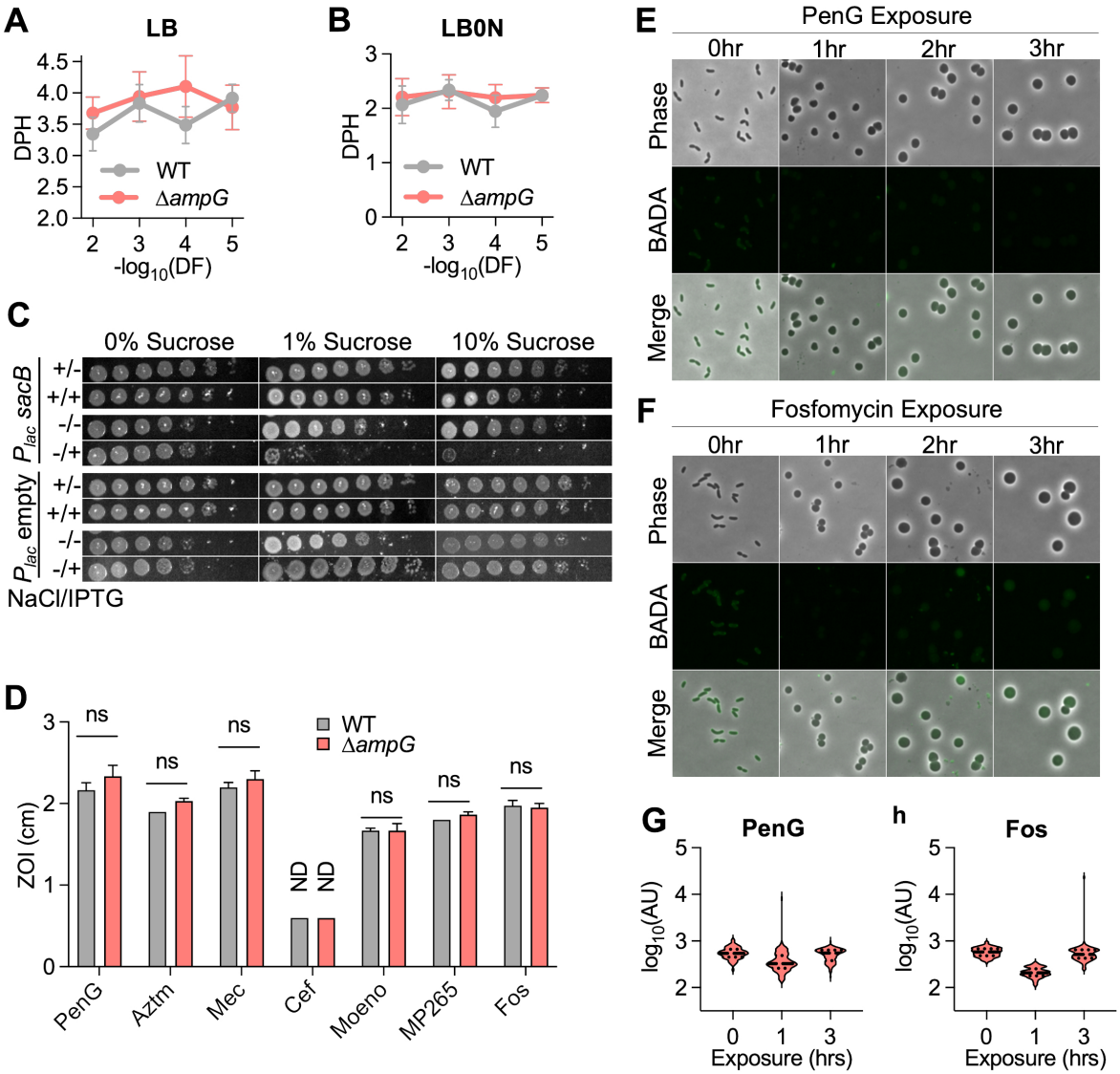

Figure 4 – Figure Supplement 3. Defects of LTG-deficient mutants are independent of PG recycling.

Δ*ampG* data for this figure was collected during the same experiments in Figures 2A and 3A-F, therefore WT data are reproduced from those figures and any statistical tests shown here were performed on the complete data sets for those experiments (including WT, Δ*ampG*, and ΔLTG strains). **(A-B)** Mass doubling times from growth curves performed in LB or LB0N inoculated with 10-fold serial dilutions (10^0-10^{-6}) of saturated overnight cultures. Error bars represent standard deviation of the mean, n≥3. **(C)** Saturated overnight cultures harboring IPTG-inducible *sacB* or empty vector were 10-fold serially diluted (10 and plated on LB+kan50 and LB0N+kan50 +/- IPTG (200μM) +

sucrose (0, 1, or 10% W/V) and incubated at 30 °C for 24 hrs before imaging. Representative of 3 biological replicates. **(D)** Sensitivity to Penicillin G (PenG), aztreonam (AZTM), mecillinam (Mec), cefsulodin (Cef), moenomycin (Moeno), MP265, and Fosfomycin (Fos) measured as Zone of Inhibition (ZOI) in a disk diffusion assay. ND = No ZOI around disk. Error bars = standard deviation. Significance determined by one-way Anova. ns = p>0.05. Overnight cultures were diluted 1:100 into LB+BADA (100μM) and grown at 37°C to OD_{600}0.5 before addition of **(E)** PenG (100μg ml^{-1}) or **(F)** Fosfomycin (500μg ml^{-1}). Samples were washed and imaged after 3hrs of antibiotic exposure. Fluorescence was normalized to the same intensity threshold as Figures S12 and S13 for comparison. Representative of 2 biological replicates. Scale bar = 5μm. **(G-H)** Mean fluorescence intensity (AU) for >100 BADA-labeled cells or spheroplasts were measured in ImageJ.

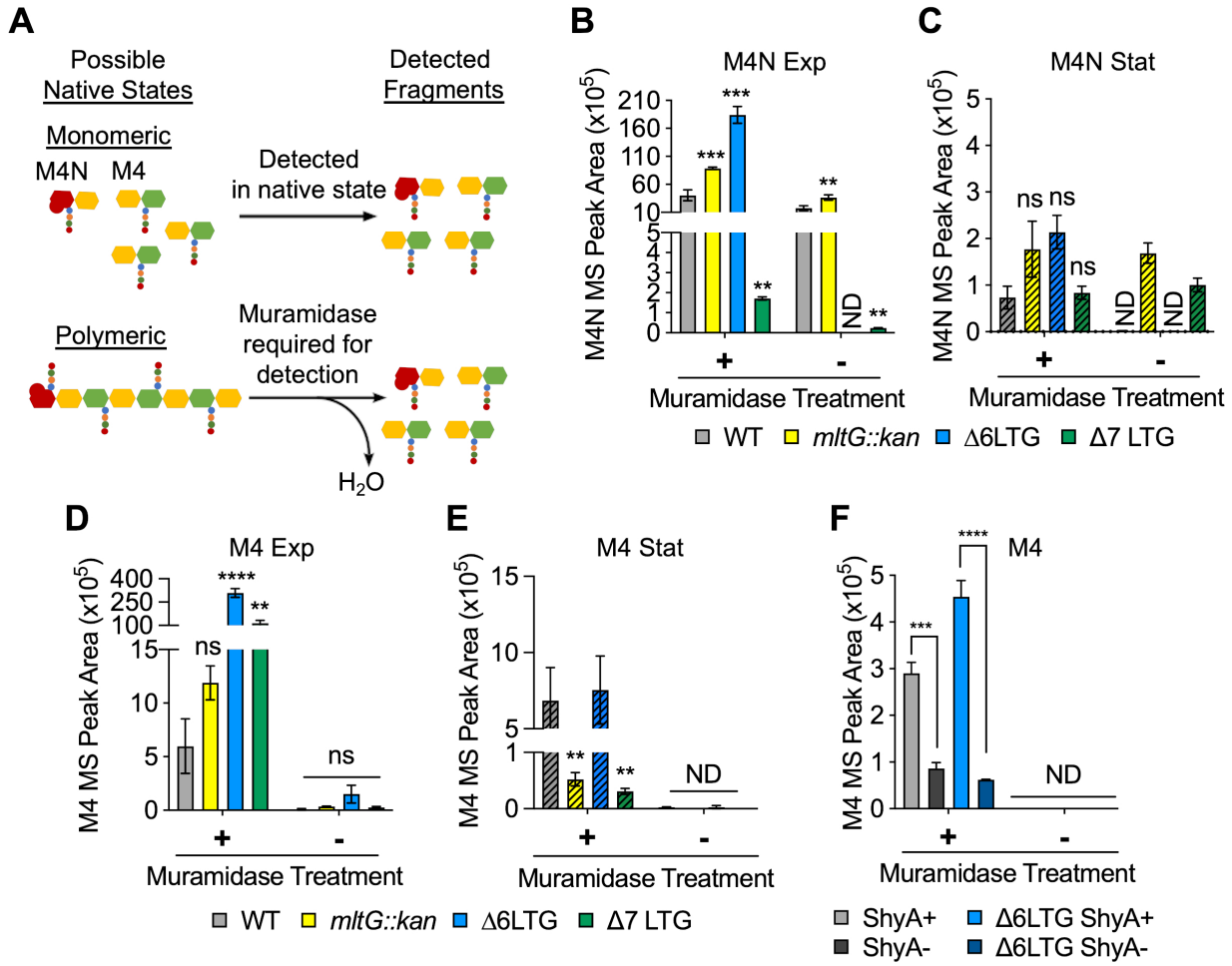

Figure 5. Periplasmic uncrosslinked PG strands accumulate in an endopeptidase-dependent manner during normal growth

(A) Schema describing muramidase-treatment dependence of detection of monomeric or polymeric PG fragments. M4N = anhMurNAc-tetrapeptide. M4 = reduced MurNAc-tetrapeptide. **(B-E)** Overnight cultures of. WT and ΔLTG mutants were diluted 1:100 into

LB, grown at 37°C, and harvested at OD_{600} 0.3 (Exp, solid bars) and 1.2 (Stat, striped bars) for soluble PG analysis by LC-MS. MS peak areas for M4N and M4 are shown here and complete muropeptide profiles can be found in Supplemental File 2. Means compared to WT by unpaired t-tests, n=3. **(F)** WT and Δ6 LTG strains harboring a single chromosomal copy of *shyA* under an IPTG-inducible promoter were grown from 10^{-2} inocula for 3hrs (OD_{600} ~1.0) in LB with (ShyA+) or without (ShyA -) 200μM IPTG at 37 °C and harvested for soluble PG analysis by LC-MS. Complete muropeptide profiles can be found in Supplemental File 3. Means compared by unpaired t-test, n=3. All error bars = standard deviation. ns = p>0.01, ** = p<0.01, *** = p<0.001, **** = p<0.0001. ND = Not detected in all replicates.

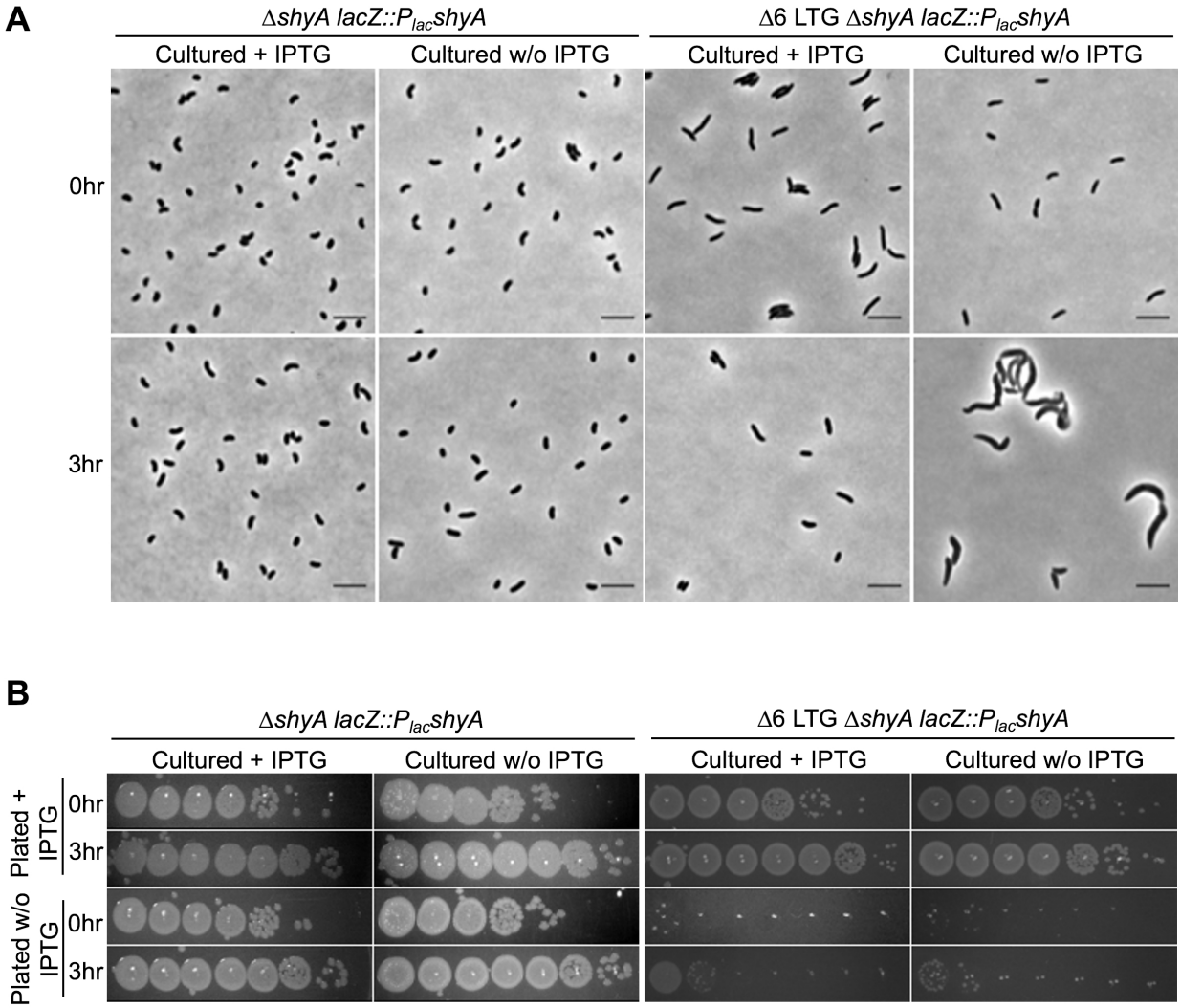

Figure 5 – Figure Supplement 1. Endopeptidase depletion phenotypes in LTG-deficient mutants.

WT and Δ6 LTG strains harboring a single chromosomal copy of *shyA* under an IPTG-inducible promoter were grown from 10^{-2} inocula for 3hrs (OD_{600} ~1.0) in LB +/- IPTG (200μM) at 37 °C. Samples were **(A)** imaged on LB + agarose pads and **(B)** spot plated

in 10-fold serial dilutions (10^0-10^{-6}) onto LB+/- IPTG (200μM), then incubated at 30 °C for 24hrs before imaging. Representative of 3 biological replicates.

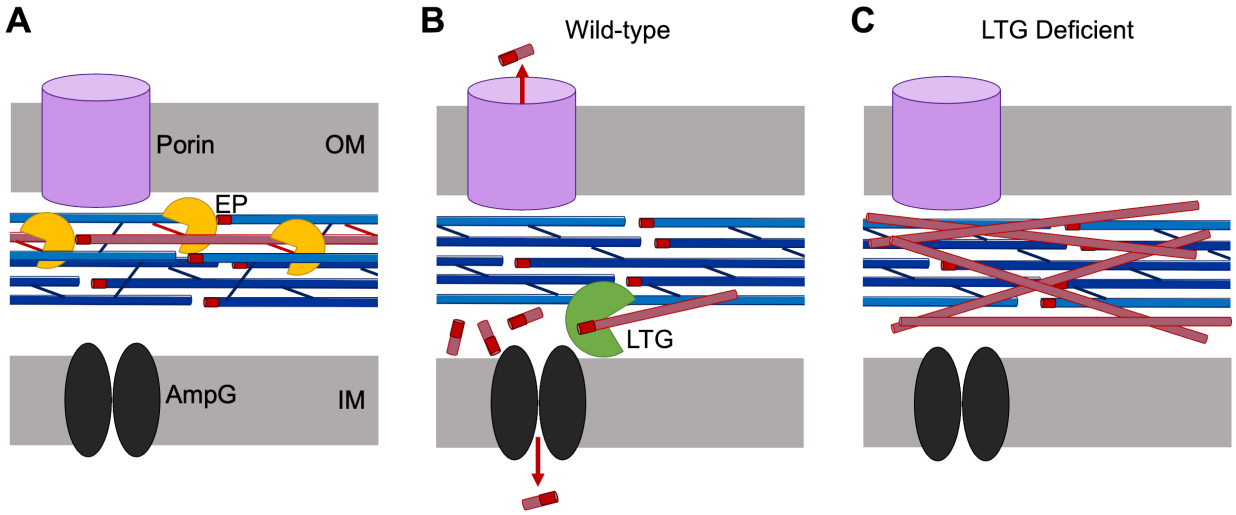

Figure 6. Model for LTG-mediated removal of toxic PG debris
(A) Endopeptidases (EPs, Yellow) excise PG strands (Red) from the sacculus (Blue), permitting sacculus expansion. **(B)** In wild-type cells, lytic transglycosylases (LTGs, Green) digest excised, uncrosslinked PG strands into smaller fragments that can be recycled by AmpG (Black) or released through porins (Violet) **(C)** In LTG deficient cells, excised PG debris crowds the periplasm and becomes toxic.

Supplemental File 1. Complete sacculus muropeptide composition profiles of LTG-deficient mutants
Supports Figure 1 – Figure supplement 1D. Presents mean relative muropeptide abundance +/- standard deviation of the mean for all detectable muropeptide species from muramidase-treated sacculi isolated by ultracentrifugation from LTG-deficient mutant cultures during exponential and stationary growth phases. n = 3.

Supplemental File 2. Complete muropeptide detection profiles of soluble PG material from LTG-deficient mutants
Supports Figure 5BCDE. Presents mean mass peak area +/- standard deviation of the mean for all soluble, detectable muropeptide species from muramidase treated and untreated lysates of LTG-deficient mutant cultures during exponential and stationary growth phases. n = 3.

Supplemental File 3. Complete muropeptide detection profiles of soluble PG material from ShyA-depleted mutants
Supports Figure 5F. Presents mean mass peak area +/- standard deviation of the mean for all soluble, detectable muropeptide species from muramidase treated and untreated lysates of cultures grown with and without ShyA induction. n = 3

1237

1238 **Supplemental File 4. Bacterial strains, plasmids, and primers used in this study**